Green Open Access added to TU Delft Institutional Repository

'You share, we take care!' - Taverne project

https://www.openaccess.nl/en/you-share-we-take-care

Otherwise as indicated in the copyright section: the publisher is the copyright holder of this work and the author uses the Dutch legislation to make this work public.

Cement and Concrete Research 185 (2024) 107649



Contents lists available at ScienceDirect

Cement and Concrete Research

journal homepage: www.elsevier.com/locate/cemconres



On the micro- and meso-structure and durability of 3D printed concrete elements

Kim Van Tittelboom [a,*], Manu K. Mohan [a], Branko Šavija [b], Emmanuel Keita [c], Guowei Ma [d], Hongjian Du [e], Jacques Kruger [f], Laura Caneda-Martinez [c], Li Wang [d], Michiel Bekaert [a], Timothy Wangler [g], Zhendi Wang [h], Viktor Mechtcherine [i], Nicolas Roussel [c]

[a] Ghent University, Department of Structural Engineering and Building Materials, Belgium
[b] TU Delft, Faculty of Civil Engineering and Geosciences, the Netherlands
[c] Gustave Eiffel University, Navier Laboratory, France
[d] Hebei University of Technology, China
[e] National University of Singapore, Department of Civil and Environmental Engineering, Singapore
[f] Stellenbosch University, Department of Civil Engineering, South Africa
[g] ETH Zurich, Department of Civil, Environmental and Geomatic Engineering, Switzerland
[h] China Building Materials Academy, China
[i] TU Dresden, Institute of Construction Materials, Germany

ARTICLE INFO

Keywords:
Micro-structure
Durability
3D printed concrete

ABSTRACT

3D printed concrete (3DPC) creates opportunities, including a reduction in construction waste and time and increased design freedom. However, because of the differences in the construction technique compared to traditional concrete casting, the structures also perform differently; namely, the micro- and meso-structure and durability are shown to be different. For the 3DP technology to find its way to the market, one needs to be aware of these differences and needs to know how to quantify the above-mentioned properties, as differences in the testing methodologies impose themselves when characterizing printed instead of cast concrete. In this paper, we elaborate on the test methods to investigate the micro- and meso-structure and the durability of 3DPC. We start with a discussion on the micro- and meso-structure of the 3D printed concrete and how it is different from conventional mold-cast concrete. An in-depth discussion of the test methods to assess the durability of 3D printed concrete is outlined. Reported findings related to the two aforementioned properties are discussed. In addition, we report on the technologies proposed to improve the durability performance of 3DPC, and we highlight the remaining challenges and opportunities related to 3DPC.

1. Introduction

Concrete durability can be defined as its ability to resist weathering, chemical attack, abrasion, or any other process of deterioration [1] during its designed service life. This holds in the case of 3D printed concrete (3DPC) elements. However, micro- and meso-structure and, consequently, the durability of 3DPC structures differ in several respects from those of (pre)cast reinforced concrete, forcing us to take one step back when considering durability. In the case of (pre)cast reinforced concrete, we usually design new structures for durability based on a standardized [2] prescriptive approach. According to this approach, the resistance of structures to environmental impacts is considered to be assured when specific requirements are met. Depending on the exposure class, requirements for concrete strength class, water-to-cement (w/c) ratio, cement content [2], cover depth, and crack width [3] are defined as 'guarantying' the required service life without the need for any durability tests before construction and any significant repair actions after its completion. For more innovative concrete solutions, the standardized prescriptive approach is not valid, and we design for durability according to the performance-based approach [4,5]. This implies the execution of performance tests and the use of prediction models to prove that acceptance criteria are met and that the required service life will be attained. Thus, the application of a performance-based concept requires reliable performance test methods and sound models based on scientific

* Corresponding author.
E-mail address: kim.vantittelboom@ugent.be (K. Van Tittelboom).

https://doi.org/10.1016/j.cemconres.2024.107649
Received 22 February 2024; Received in revised form 20 August 2024; Accepted 20 August 2024
Available online 27 August 2024
0008-8846/© 2024 Elsevier Ltd. All rights are reserved, including those for text and data mining, AI training, and similar technologies.

understanding [6] of the relevant mechanisms and phenomena. While the performance-based concepts facilitate the first steps in the durability design of innovative 3D printed elements, it is obvious that prediction models will become more complicated when adapted to layered, i.e., anisotropic and less homogenous 3D printed structures. Furthermore, conventional test methods to measure the ingress of aggressive agents will need to be modified because of the peculiarities of 3DPC elements.

These peculiarities can be grouped into *material-related*, *process-related,* and *geometrical* issues (Fig. 1). This should be explained here using the example of extrusion-based 3D printing, which is, by far, the most common 3DPC approach used today, both in research and practical applications. Therefore, the scope of this article is limited to extrusion-based additive manufacturing methods. Focusing first on the *material-related* differences, concrete materials used for 3D printing commonly contain smaller-sized aggregates (mostly D_{max} equals 1–2 mm, while only a handful of studies report larger D_{max} values of 4 mm to 20 mm [7,8]) and higher binder contents (binder contents of 600–1000 kg/m^3 have been reported [9,10]), compared to traditional cast concrete. These specifics can be traced back to the efforts to enable a problem-free processing of the fresh material through the pipeline and nozzle. The limited grain size would, according to some definitions, force us to speak about 'mortar' instead of 3D printed 'concrete'. However, in the context of structural applications, '(fine-grained) concrete' would indeed be the correct term [11]. For the sake of simplicity, we will use the term 'concrete' throughout this article independent of the maximum aggregate size. In addition, admixtures such as accelerators are frequently added to 3D printable mix compositions to increase the structural build-up rate. All of these *material-related* aspects are specific for 3D printed concrete, i.e., smaller-sized aggregates, higher powder contents, and the addition of accelerators, potentially increasing the risk of shrinkage cracking depending on their chemical nature. So, models treating the concrete as a continuum and ignoring the presence of cracks are expected to deviate from reality more than cast concrete.

Among the *process-related* issues, we want to highlight the fact that the 3D printed material is extruded from a nozzle, and there is a lack of compaction during and after material deposition. This causes variations in the micro- and meso-structure depending on the extruded concrete composition, the rheological properties of the mixture, the age of the mix at deposition, and the extruder parameters [11]. Another difference compared to cast concrete, which results from the *process*, is the fact that we end up with anisotropic layered structures, which may exhibit considerably higher porosity in the interlayer region than in the filaments themselves. Parameters defining whether or not these interlayers need to be considered as weak zones are the time gap between the deposition of two layers in relation to the setting time of the mixture, the local pressure applied to increase interlayer compaction by the nozzle, the number of layers on top of the considered interlayer, etc. Thus, 3DPC is anisotropic and more heterogeneous in comparison to cast concrete. Furthermore, even for monolithic cast concrete, it is already debated that the size effect should be taken into account in durability testing since larger samples show a lower critical chloride content than small samples under identical exposure conditions [12,13]. This effect is likely to be more pronounced for 3D printed samples. In layered printed samples, the pressure acting on the bottom layers and the subsequent degree of compaction can differ considerably in smaller-scale samples compared to larger ones or structures themselves. In addition, for 3D printed elements, the ingress of aggressive agents will vary in different directions and will need to be tested in relation to the printing path and layer orientation. The last *process-related* difference between cast and printed concrete we would like to address is the lack of formwork in the 3D printing technology. While this will affect the required material properties (thixotropic mix compositions with high yield stress and fast setting are required), an important consequence is a high vulnerability to drying shrinkage at very early ages and related cracking, as well as an increase in the porosity of printed concrete.

Finally, printing instead of casting an element also causes some *geometrical* issues. The layering of 3D printed elements influences the meso-structure and results in the fact that large voids could be enclosed between filaments placed on top of or deposited next to each other, forming preferential ingress paths for aggressive agents. The frequently bulged shape of filaments and relatively high surface roughness increase the exposed surface area, which compromises the resistance against the ingress of aggressive media. Next to the additional voids and interfaces between layers, in the case of stay-in-place formwork printing, the additional interface between printed formwork and infill material needs to be considered as well. Depending on the microstructure of the

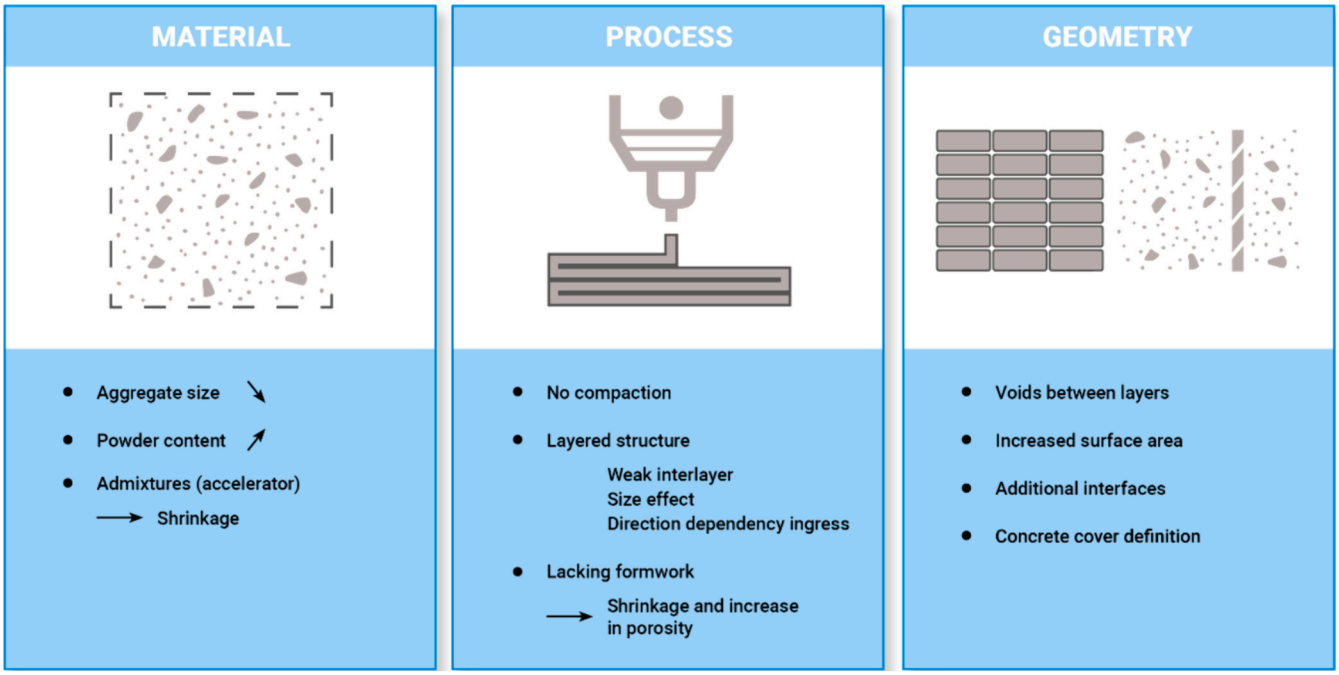


Fig. 1. Material-related, process-related and geometrical issues in 3DPC.

material next to the printed formwork and depending on the meso-structure of the printed formwork (which could cause the inclusion of air gaps as a result of the surface roughness or the irregular bulged shape of filaments), additional preferential ingress paths occur. Furthermore, in traditionally cast reinforced concrete, the concrete cover is specified as the least distance between the surface of the embedded reinforcement and the outer surface of the concrete. However, for 3D printed concrete, if reinforcement is used the specification of the concrete cover is less straightforward. Which surface should be considered as the outer surface? Can the printed formwork itself be taken into account? On the one hand, high-quality materials with high binder contents are used, so it would make sense to consider the printed layer(s) as a part of the cover. On the other hand, due to the presence of weak interlayers, they could cause preferential ingress. As surfaces are not flat but bulged (for both the infill material and the printed formwork), the distance between the rebar and the 'outer surface' also varies over the rebar length, which is another aspect that complicates the definition of the concrete cover in case of 3D printed reinforced elements.

All of the before-mentioned *material-related*, *process-related,* and *geometrical* issues specific to 3DPC clearly affect the micro- and meso-structure and thus have a significant effect on the durability performance of 3DPC. This means that performance testing becomes more complicated. This will be one of the topics to be further elaborated in this paper. In Section 2, we will first discuss the test methods that could be used to evaluate the micro- and meso-structure of 3D printed elements. We will also summarize the findings related to the micro- and meso-structure specific to 3D printed materials. In Section 3, a similar approach will be followed: we will first discuss the specific test methods to test the durability of 3D printed elements, after which we will present the findings related to the durability. Durability tests considered in this paper are water absorption tests, water and oxygen permeability tests, carbonation and chloride ingress tests, freeze-thaw tests, sulfate and (sulfuric) acid attack, and abrasion as well as durability-related tests such as shrinkage tests and exposure to elevated temperature. It will be stressed that designers should understand basic deterioration mechanisms and potential types and rates of damage. As from Sections 2 and 3, it will become clear that testing does not only become more complicated but that durability might also be compromised in the case of 3D printing, mainly because of the layering and the lack of formwork and related shrinkage and cracking. However, we will demonstrate in Section 4 that there are still multiple ways of further improving the situation and increasing the durability performance of 3D printed elements. In the last section, i.e., Section 5, we will discuss challenges to be further tackled in the future to successfully implement 3D printing in the practice of construction while securing the designed service life.

Note that in this paper, we will discuss generic concepts of the durability of 3D printed materials. Although we are well aware that the intended application will have an impact on the durability requirements, we will consider in this paper both structural and non-structural applications, being reinforced (with steel bars in infill or printed materials or with (steel) fibers) and non-reinforced (compression only structures). Of course, depending on the exposure class and the targeted application, not all requirements will have to be fulfilled.

2. Micro- and meso-structure

Changes in the *material* composition of 3DPC compared to cast concrete will logically result in changes in the micro-scale level, also called cement paste level (consisting of capillary pores plus C-S-H matrix, CH crystals, and clinker phases). The aforementioned *process-related* and *geometry-related* peculiarities of 3DPC will mainly impair the meso-scale level, including the mortar/concrete level (cement paste plus aggregates and interfacial transition zone (ITZ)) and sample level (consisting out of interlayers but also containing shrinkage cracks and defects). The analysis of 3DPC in terms of its micro- and meso-structure must, therefore, involve the examination of the bulk concrete, the interlayer region, and their combined effect.

2.1. Test methods to evaluate the micro- and meso-structure of 3D printed elements

2.1.1. Global methods

When it comes to studying the micro- and meso-structure of 3DPC, porosity represents one of the main parameters of interest. In this regard, vacuum saturation and mercury intrusion porosimetry (MIP) are the most widespread techniques to study the global porosity of concrete, although they present limitations when it comes to distinguishing between the contribution of the bulk and the interlayer region.

A handful of studies determined the porosity of 3DPC with the vacuum saturation method [14–18]. Rahul et al. [16] extracted 20 × 10 × 10 mm^3 3DPC specimens with and without interlayer region in the middle mainly to capture the interlayer porosity. Meanwhile, others used specimens with multiple layers and did not distinguish between the porosity of the bulk and interlayer region. The specimens were initially dried in an oven, followed by several hours in a vacuum desiccator to eliminate surplus moisture and equilibrate with room temperature. Subsequently, the samples were submerged in water within the desiccator while maintaining the vacuum. After an hour, the vacuum was released, and the specimens remained submerged in the solution. By measuring the hydrostatic weight and the saturated mass, the open porosity can be calculated [17].

MIP has also been used to characterize the pore features of 3D printable materials [19–26]. This method stands out for its versatility in characterizing diverse pore sizes. Yet, injecting pressurised mercury into the sample poses a risk of damaging the micro-structure and yielding inaccurate outcomes. In addition, sample preparation can critically affect the results obtained by MIP. This includes cutting the printed sample by mechanical means into small specimens (which must be representative of the bulk or interlayer region) and, more importantly, removing pore water before the measurement. Harsh drying methods have been reported to lead to phenomena like microcracking or decomposition of hydrates, which can artificially modify porosity, making it advisable to apply gentler methods such as solvent exchange [27–29]. Hence, meticulous attention is essential during MIP sample preparation and measurement. Another drawback of MIP tests is the potential for erroneous results caused by ink-bottle pores within the sample. Moreover, distinguishing between pores at the interlayer or within the bulk region is challenging with MIP tests.

2.1.2. Spatial methods

The preferred choice for studying the contribution of the interlayer effect in 3DPC is the use of spatial methods. These include imaging techniques like optical or electronic microscopy and X-ray micro-computed tomography (micro-CT), which allow for the direct observation of the overall micro- and meso-structure. But it is also possible to indirectly obtain spatial information by measuring and mapping a microstructure-related property, as is the case for micro- and nano-indentation, or by monitoring the penetration of external chemical agents.

2D surface analysis using an optical microscope can give porosity information of 3D printed samples and has been attempted in a handful of studies [19,30,31]. The method is generally used to capture the air voids present at the interlayer region [31]. One primary benefit of 2D surface analysis lies in its simplicity and the widespread availability of optical microscopes in most laboratories. Nonetheless, due to its limitation in offering solely a 2D surface analysis, it cannot capture the anisotropy or heterogeneity of pores [32].

In the domain of 3DPC, scanning electron microscopy (SEM) is also a widespread tool to localize and qualitatively assess the spatial heterogeneities associated with the layered deposition of concrete. As illustrated in Fig. 2, it is frequently used to observe phenomena such as air inclusion in the interlayer or the effect of drying between two

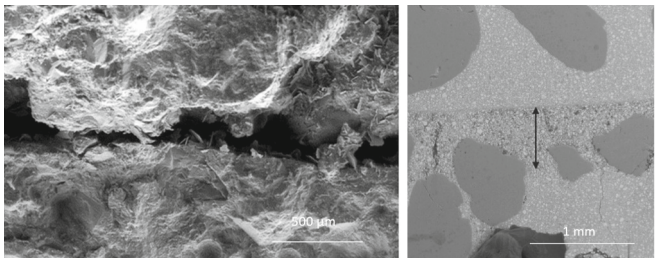


Fig. 2. Air inclusion (a) and drying (b) in the interlayer region as observed by SEM (taken from [32,36]).

subsequently deposited layers [15,32–35]. As with optical microscopy, the success of SEM is largely due to its ample accessibility in today's construction laboratories as well as its relative simplicity. Another major advantage is its high spatial resolution, which enables observations of elements over a wide range of sizes, including even the nanoscale. In addition, it is possible to complement morphological observations with energy-dispersive spectrometry (EDS) analysis to obtain data on elemental composition. On the other hand, it should be noted that the samples used for SEM analysis are typically only a few cm in size and must be split or cut (and also vacuum impregnated and polished in case of backscattered electron (BSE) imaging) from the printed element, as well as dried to be analyzed under conditions that usually involve vacuum. Therefore, SEM presents similar drawbacks to those previously mentioned for MIP in terms of representativeness and potential cracking or porosity increase associated with sample preparation [32].

The possibility of obtaining complex 3D information from the printed specimen in a non-destructive manner and with minimal sample preparation has resulted in the emergence of micro-CT as a commonplace imaging tool in the field of 3DPC. Micro-CT does not only offer a direct way to visualize microstructural features in 3D but also provides advanced quantitative information about them. Accordingly, as shown in Fig. 3, one of the most common applications in 3DPC is porosity characterization since micro-CT can provide data on pore size distribution, pore morphology (quantifiable by their circularity or aspect ratio), or connectivity and tortuosity of the pore network [15,20,30,34,37–42]. It must be taken into account, however, that the spatial resolution of micro-CT is limited to the micrometre scale and that voxel sizes between 5 and 100 µm are found in micro-CT experiments in the field of 3DPC [15,23,30,35,38,40,41,43–47]. Another valuable application of micro-CT is the localization of the interlayer region or microcracks, and examples of this are frequently found in literature [20,26,30,33–35,41–45,47–52]. It should also be noted that the non-invasive nature of micro-CT offers the possibility of carrying out time-resolved experiments, making it possible, for example, to monitor hydration/drying processes or degradation and cracking phenomena.

Regarding sample preparation, micro-CT proves to be highly advantageous as it only requires ensuring that the sample size is sufficiently small to be fully projected on the detector and that it remains steady during the analysis. This improves the representativeness of the sample and prevents any problems associated with sample drying. Nevertheless, to enhance resolution and reduce acquisition times, it is common to employ smaller specimens, which are often obtained by extraction from the printed element using techniques that can potentially damage the microstructure. In this aspect, coring (in the hardened or fresh (semi-solid) state) is frequently performed, as it provides cylindrical samples, which is the most efficient geometry for micro-CT [53].

Recently, some studies started to spatially investigate the microstructure of 3DPC using micro- or nano-indentation techniques [43,54,55]. In general, these studies focus on the location and fine characterization of the interlayer region by measuring micromechanical

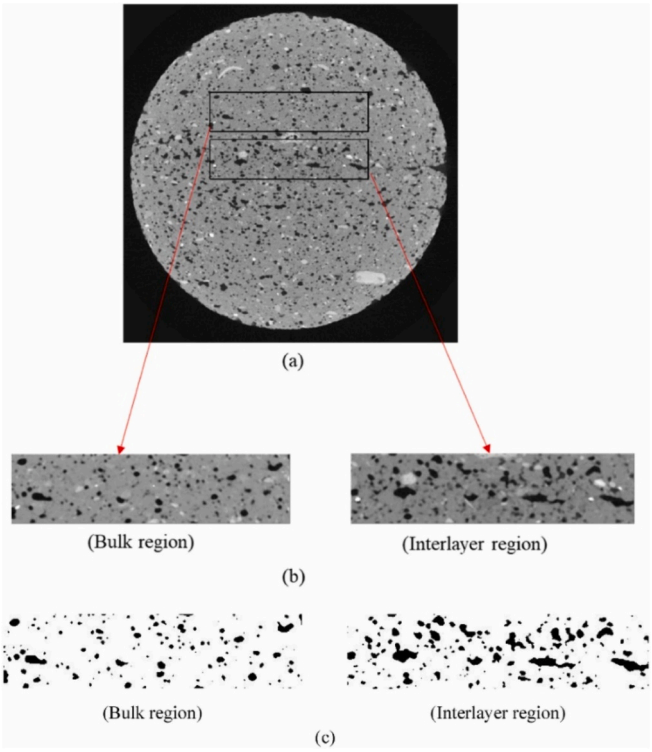


Fig. 3. Study of the porosity in the bulk and interlayer region by micro-CT: (a) slice from the 3D tomographic reconstruction of a cylindric sample, (b) details of the bulk and interlayer region, and (c) details of the porosity in the bulk and interlayer region (taken from [20]).

parameters (usually the elastic modulus or the hardness) instead of visualizing it. This has allowed some authors to measure how the thickness (see Fig. 4) or the variation of the micro-mechanical properties in the interlayer scales with the time gap between layer depositions or the rheological properties of the material [43,55]. Moreover, Kosson et al. [56] combined the use of nano-indentation with SEM/EDX

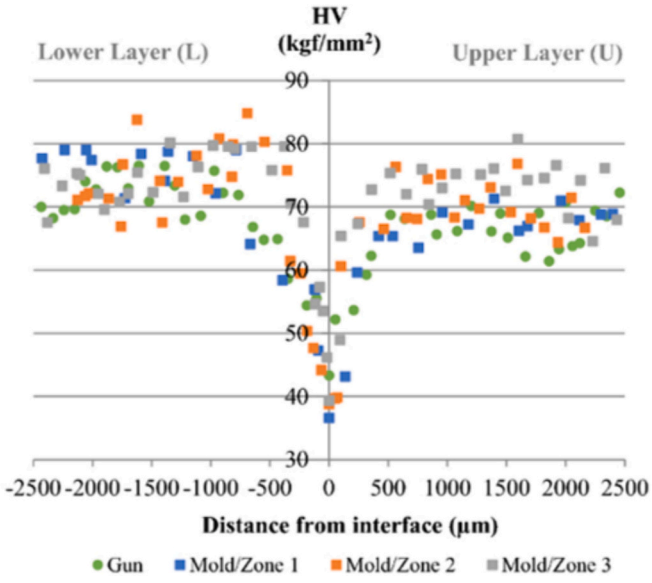


Fig. 4. Hardness value (HV) as a function of the distance from the interlayer measured on two-layered samples with a 24-hour time gap. Measurements were performed on a sample manually printed using a caulking gun ("Gun") and on three zones of a specimen printed with the caulking gun and compacted inside a mold ("Mold") (taken from [55]).

characterization to link the micromechanical response of printed materials with the mesoscale assemblage of the main hydrate phases. Given that the weakness associated with the interlayer region is a key aspect in the development of 3DPC, micro- and nano-indentation represent tools with great potential for the field. It should be noted, however, that it presents similar disadvantages to those seen in previous techniques since it requires the use of specimens of reduced size and an intensive sample treatment (cutting, grinding, and polishing) to ensure a completely smooth surface.

Methods used to measure carbonation and chloride ingress [26,34,57,58] (see Section 3) could also reveal the meso-structure of the printed concrete due to the higher interlayer ingress, as they often involve cutting the sample and performing some chemical treatment (e.g. phenolphthalein for carbonation, silver nitrate for chlorides) or direct analysis using microscopy or an elemental measurement technique such as micro-XRF [58–60]. These methods have been particularly effective in identifying nonuniform ingress (that is, non-one-dimensional ingress), which is an indication of material inhomogeneity, with more rapid ingress occurring along layer interface regions. These studies have often been carried out in the context of identifying when 'cold joints' occur by varying time intervals between layers, typically showing more rapid transport along the interface when such a 'cold joint' would form [59]. Similarly, neutron imaging (see also Section 3) experiments have also demonstrated more rapid uptake along interfacial regions, again, especially when there is a cold joint [61]. Common to all these techniques is their direct two-dimensional nature, which gives a measurable indication of porosity and other material property variation across the printed layers.

2.2. Findings related to the micro- and meso-structure specific for printed elements

2.2.1. Air voids at the interfaces and in the bulk

Because of the high consistency (or high yield stress) of printable materials, it can be expected that some air can be entrapped at the interfaces between layers. Initially, fluid materials such as the ones used in bi-component technologies are only expected to trap some small air bubbles (around 100 μm), while stiffer materials used in mono-component technologies can potentially trap millimetric air voids at the interfaces. This has been imaged using SEM [32], as shown in Fig. 2. These entrapped air voids are expected to be process-driven, i.e. they result from the trapping of air between the layers during deposition.

We moreover have to keep in mind that pumping, extrusion, or, more generally, feeding of the robot print head is a pressure-driven process, and, as such, it exposes the air bubbles inside the bulk material to pressures that may reduce their sizes. This process is expected to be reversible. However, if this external pressure is too high or is maintained for too long, the gas inside the bubbles will dissolve in the surrounding fluid. When the pressure is relieved (after deposition), new bubbles shall form. Their size distribution may, however, be different from the one reached after the primary mixing of the material [62].

As printed concrete is not vibrated, the two above features are not expected to disappear through the shaping process. These can even be enhanced by hydration, drying, shrinkage, etc., and, as such, are expected to contribute to porosity, permeability, and therefore to the durability of printed concretes.

2.2.2. Porosity induced by lack of hydration at the interface

Fresh cement-based material is deposited without any mold in the case of 3DPC. Due to the large free surface, the material may dry out extensively before setting. The amount of water that is accessible for hydration is then reduced by drying. When the initial water content is low, limited water loss caused by drying before application of the upper layer may be enough to disrupt hydration at the surface of a layer. Drying often has little impact on bulk hydration since the mass loss in the bulk material is negligible in comparison to the overall mass, but it can have significant consequences in a millimetric region near the surface or, more specifically, at the interface between two successive layers.

Furthermore, incomplete hydration in a thin crust may result in excessive local porosity and weak mechanical properties at the layer interface. According to Keita et al. [36] the initial w/c affects the interfacial strength between two layers of mortar. The interface strength is equal to the bulk set material for high w/c, but it is reduced for w/c ratios below 0.35. Additionally, a crust forms. The reason for dried crusts at the free surface is that the material's internal water flow is unable to meet the evaporative demand as a result of the initial drying flux at the surface. Suction causes a liquid flow inside the porous structure when water evaporates. If the water flow inside the substance moves quick enough, the water that evaporates is compensated, the material maintains its homogeneity and the cement hydrates uniformly. For classic concrete applications, this is typically the situation.

However, printed concrete temperature and environmental factors (wind, humidity, ambient temperature and solar radiation) can greatly affect the evaporation rate. Because of extrusion friction and the addition of accelerators to the mixture, the temperature of cementitious materials produced by 3D printing may rise above 25 °C. As a result, the drying rate could rise from the one at room temperature by a factor of up to 100 [63]. Thus, a thin crust is likely to form at the free surface of a 3D printed layer if the drying rate is fast and the ability of the material to adjust to this rate it is limited. It may then result in poorly hydrated, porous surfaces, as depicted in Fig. 2.

2.2.3. Modification of porosity

In terms of porosity, literature generally agrees that the porosity of 3DPC seems to increase compared to cast concrete. For instance, Rahul et al. [16] revealed that the interface region exhibited a vacuum-saturated porosity being 10–16 % higher compared to cast samples made with the same concrete composition, while bulk-extracted samples displayed a slightly lower porosity. Bekaert et al. [17] investigated the effect of curing conditions on the vacuum-saturated porosity of 3DPC and reported that open porosity becomes lower when the relative humidity during curing is higher. Several micro-CT studies reported results with the same trend, showing higher porosity in the 3D printed interlayer region compared to the bulk matrix [45,64,65]. This effect is correlated to the time gap between layer deposition, as demonstrated by Van Der Putten et al. [66] and pore size distribution was similar across various areas of a printed element. However, with longer time gaps ($\geq$10 min), the number of pores increased not just at the layer interface but also within the layer itself. In contrast to the findings frequently reported for mono-component mixtures, a recent study revealed that, in the case of 3DPC with bi-component mixtures, the total porosity could be lower than the value measured for mold cast counterparts [22]. In addition to the higher total porosity, the shape and size of the pores can also be affected. Mohan et al. [20] assessed the porosity and pore features, such as tortuosity and pore complexity, using MIP testing and observed that the interlayer regions have larger and interconnected pores with low tortuosity. The authors also reported that the aspect ratio of pores at the bulk region falls within the 1–1.6 range, suggesting spherical or equally sized pores in all dimensions within this region. Conversely, regardless of the time gap, all samples exhibited significantly higher average aspect ratios (>3) within the interlayer region, indicating predominantly elongated pores. Chao Liu [5] highlighted differences in pore distribution between layers and the bulk matrix of 3DPC, emphasizing flatter, longer pores compared to traditional cast concrete, with the anisotropic directional distribution. Elongated pores in the interlayer area have also been recently noted by other researchers [19,30,41]. The increased overall porosity and prevalence of elongated pores in the interlayer zone might stem from reduced compaction between freshly deposited concrete layers during the printing process.

Another aspect that should be taken into account is that the printing process parameters can significantly influence the porosity of 3DPC. In the 3D printing process, the material undergoes pumping and then

deposition, where pressure loss can be high depending on the rheological properties of the material. Due to the high pumping pressure, the printed material can have a very different pore distribution compared to the mixing stage [62]. In addition, early-age drying (depending on the environmental conditions) can impact the porosity and micro-structure of the printed element. Recently, Mohan et al. [67] reported that the total porosity and critical pore diameter significantly increase if the samples are subjected to early-age drying. Also, the authors reported that the total porosity and critical pore diameter can be lowered with the addition of a reducing agent as it reduces the rate of water loss due to evaporation by increasing the viscosity and reducing the surface tension of the pore solution [67–71]. Rahul et al. [72] examined the effect of drying on the micro-structure with SEM imaging. For both dried and undried samples, a higher porosity was observed in the regions very close to the aggregate surface due to a limited amount of anhydrous particles close to the aggregate surface. Samples undergoing drying were found to have a significantly higher porosity in the ITZ and also in the bulk regions away from the aggregate surface. Early-age drying could also cause damage to the micro-structure of the system and could result in durability issues later.

2.2.4. Micro-cracking in the bulk

Many factors may induce the formation of cracks inside the material and thus influence the meso-structure. Some of these factors are well-known and have been extensively studied for concretes shaped using standard casting technologies. These are reported to originate from chemical shrinkage along with autogenous shrinkage and are both expected to happen some hours after casting. Some other factors specific to 3D printing may induce micro-cracking at earlier stages.

First, printable materials have fresh properties that strongly differ from cast concretes, which is one of the *material-related* issues mentioned before in 3DPC. Such materials are considered to behave as jammed concentrated suspensions, in which shear localizes in a region of thickness decreasing with the solid fraction [73]. For high solid fractions and strong particle interactions, this localization can ultimately lead to a cracking behaviour very similar to the ones observed for fragile solids. In the case of concrete printing, this behaviour was reported to relate to printing lace curvature and, more generally, to the potential presence of tensile stresses in these fresh, stiff materials. It was reported in [74] that small radii of curvature in the nozzle path may result in tearing and/or cracking of the outer edge of the material.

Moreover, drying of the material in the absence of a formwork is affecting the micro-structure as described above, potentially preventing complete hydration. But it is moreover expected to be at the origin of some capillary stresses. These stresses should overall lead to a contraction of the material but the printed material is restrained in many ways. First, it is in contact with stiffer layers below or even with a rigid substrate. This shall limit the freedom of the material to contract and turn contraction strains into stresses. These stresses can locally become tensile stresses and lead to the propagation of microcracks at the level of the layer itself. Second, at a more local microstructural level, because of the strong interaction between grains, some particles are expected to be prevented from rearranging. This may lead to heterogeneities in the stress and strain field that may, in turn, lead to some localized microcracking.

3. Durability

3DPC behaves strikingly different from conventional cast concrete in terms of micro- and meso-structure as explained in detail in the previous section. Due to the anisotropy and heterogeneous nature, the existing durability assessment methods may not be directly applicable to 3DPC. In addition, lack of formwork protection and the resulting early-age drying induce irreversible changes, which can have an impact on long-term durability. In this section, we provide an overview of the test methods to assess the durability of 3DPC and the adaptations needed. Also, the main findings related to the durability of 3DPC reported in the literature are summarized.

3.1. Test methods to evaluate the durability of 3D printed elements

3.1.1. Water absorption

While water ingress itself is not harmful to concrete, water acts as a medium for the transport of aggressive substances, which renders water transport a suitable measure to assess the durability of 3D printed concrete. Water sorption could be measured through the standard gravimetrical test method based on NBN EN 13057 [75], as was done by Van Der Putten [76]. Therefore, cylindrical or prismatic samples were drilled from or sawn out of linear printed elements consisting of at least one interlayer (see Fig. 5). Afterwards, samples were dried in an oven, and the sides were covered with tape or coating to ensure unidirectional water ingress. Subsequently, samples are brought into contact with water, either the water exposure surface as front or bottom (see Fig. 5). The mass increase is measured, which allows us to calculate the water uptake over time and the sorption coefficient when the exposure surface area is taken into account.

However, one question that might be raised is how to define the exact exposure surface area in the case of a curved surface, which is typical for 3D-printed concrete. Moreover, while the gravimetrical measurements in the water sorption test are easy to perform, the test results give no information on the spatial water distribution in the 3D printed sample. Knowing that the water ingress in printed samples will not occur uniformly and lacking the possibility to visualize the effect of the interlayer, these are major drawbacks of this test method. One option, which has also been applied by Van Der Putten to visualize water ingress in printed concrete, is to perform neutron radiography measurements while test samples undergo a sorption test. This allowed visualization of the movement of the waterfront in time and demonstrated the position and the effect of the interlayer. Moreover, as can be seen from the below radiographs (see Fig. 6), not only does the presence of the interlayer cause the non-uniform water ingress, but there are also differences in the water ingress rate when the bulk of the layers and the outer sides of the layers are compared. This underlines the importance of preparing test samples for which the curved outer surfaces remain present. Zhang et al. [65] utilized X-ray tomography combined with the CsCl enhancing method to assess the behaviour of water transport along the different interlayer zones of 3D printed concrete compared with cast concrete. The authors observed that due to the presence of the interlayer region, water transport was faster in 3D printed concrete compared to cast concrete [65].

3.1.2. Gas permeability

In addition to the water permeability testing discussed before, the gas permeability (mainly using oxygen gas) of printed samples could be measured to estimate the transport properties. There are only a handful of studies that focused on the gas permeability. Van Steenkiste and Wauters [77] were inspired by the CEMBUREAU method to perform gas permeability tests on printed concrete samples. The sample preparation procedure had to be adapted to suit the layered composition and anisotropic behaviour typical for printed concrete. Samples were prepared from printed linear wall elements, out of which 50 mm diameter cylindrical samples were drilled orthogonal to the print direction. Assuring that samples would fit perfectly in the test setup, the curved sides were sawn off, and cylinders with a height of 50 mm were obtained. This latter processing step could already raise the question of whether sawing off the curved sides will have a major influence on the obtained test results. After measuring and drying, samples were glued with epoxy into 50 mm high concrete rings with an outer diameter of 150 mm and inner diameter of 70 mm, which were coated to become impermeable. As such, samples fitting perfectly in the pressure cell of the CEMBUREAU permeameter were obtained. Subsequently, the gas permeability was measured using the same procedure as for cast concrete. Also, Mustapha

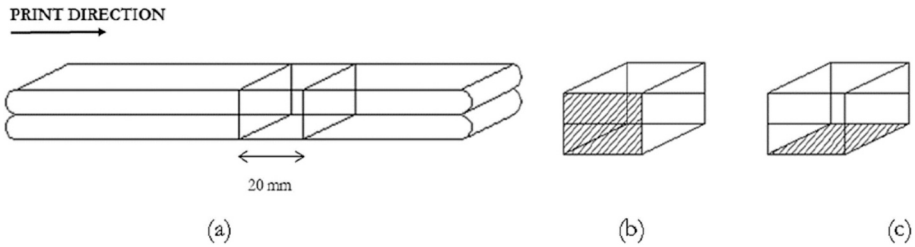


Fig. 5. Schematic depiction of the water exposure surfaces: (a) the original printed sample, (b) the 'front' water exposure surface, and (c) the 'bottom' water exposure surface (taken from [76]).



Fig. 6. Visualization of water uptake in a 3D printed sample (a) with side surface exposed and (b) with bottom surface exposed (taken from [76]).

et al. [78] reported the gas permeability tests done on 3DPC. They performed the test as described in SANS-3001-CO3-1-2 [79,80]. Cylindrical specimens were obtained from printed elements in two different directions, which include vertically cored cylinders perpendicular to the printing direction and horizontally cored cylinders perpendicular to the printing direction. The specimens were oven-dried and then placed in a compressible collar (see Fig. 7a) within the rigid sleeve, which was subsequently placed on top of a permeameter cell (see Fig. 7b). The pressure in the permeameter was increased to 100 ± 5 kPa. The time was recorded until the pressure dropped below 50 kPa.

3.1.3. Carbonation

As the carbonation of concrete structures takes a significant amount of time before detection, accelerated carbonation tests are highly favoured. The acceleration of the carbonation process is related to the increased CO_2 level within the test setup. While a normal environment has a CO_2 concentration of 0.03 % - 0.1 %, carbonation closets can realize concentrations between 1 % and 100 % [81]. While the accelerated test is favoured for the reduction in test time, both over- and underestimations of the carbonation rate are typically made with respect to the natural carbonation [82]. For 3D printed concrete, only accelerated tests have been reported. Van der Putten [83] and Malan et al. [57] performed the accelerated test at lower CO_2 concentrations (1 % and 2 %, respectively), while Zhang et al. [26] and Sanchez et al. [58] used higher CO_2 concentrations (20 % and 50–90 %, respectively).

The carbonation resistance is highly affected by the tested concrete specimens' relative humidity (RH). While a high RH in concrete leads to water blocking the ingress of CO_2, a low RH results in insufficient presence of moisture to form calcium carbonate. The lowest carbonation resistance is expected at an internal RH of around 60 % [84]. Therefore, the preparation and curing method can have a significant effect on the obtained carbonation results. Malan et al. [57] cured their printed specimens for 28 days at a relative humidity of 65 ± 5 %. The accelerated carbonation test was performed under the same RH conditions. Van der Putten [83] cured the samples and performed the test under the same RH conditions but reduced the curing period before testing to 12 days. Zhang et al. [26] cured the printed specimens at a relative humidity of 95 ± 5 % for 26 days and dried the specimens for 48 h at 60 °C before testing. The specimens were tested under an RH condition of 70 %. Sanchez et al. [58] cured printed samples under 'ambient' conditions for two months before testing at an RH of 70 %.

For conventional cast concrete specimens, the carbonation rate can be easily defined by measuring the distance between the carbonation front and the exposure surface. In the case of printed concrete, the printed surface is bulged, which leads to a two-dimensional ingress. At this point, the question becomes how to determine the ingress depth. Is the outer surface the reference point, or should an equivalent surface be determined based on the overall curvature of the printed element? Zhang et al. [26] measured the carbonation ingress along the exposed surface at different positions every 10 mm along the total height of the samples (layer thickness: 12–15 mm). Malan et al. [57] determined the



Fig. 8. Determining carbonation ingress depth on (a) mold cast and (b) printed concrete samples (taken from [57]).



Fig. 7. Oxygen permeability apparatus (a) compressible collar (b) permeameter cell (taken from [78]).

ingress at the position of the bulges and the position of the layer interfaces (layer thickness: 10 mm) by means of a calliper (see Fig. 8). Van der Putten [83] reported the ingress depth based on image analysis, by which the ingress depth was measured every 1 mm (layer thickness: 10 mm). All researchers defined the ingress depth as the horizontal distance between the exposure surface and the carbonation front, as indicated by the colour change boundary of the phenolphthalein.

3.1.4. Chloride ingress

As described in the introduction, 3DPC may show an increased porosity at the interlayer and frequent shrinkage crack formation, both of which are weak zones susceptible to faster ingress of chlorides. Therefore, these aspects must be considered when assessing the resistance of 3D printed concrete to chlorides, and this makes specimen preparation of critical importance. This includes the number of printed layers, extraction of test specimens, direction of chloride exposure, and testing procedure. In general, multilayer specimens have been tested. Several studies used prismatic specimens for chloride testing: Van Der Putten et al. [34] printed four-layered beams (300 mm long) and cut smaller ($40 \times 40 \times 33$ mm^3) specimens for chloride testing. Bran-Anleu et al. [59] printed three-layered walls ($1200 \times 30 \times 60$ mm^3) and cut out specimens with dimensions of $40 \times 10 \times 25$ mm^3 after hardening. Malan et al. [57] 3D printed beams and extracted smaller prismatic samples 30 min after printing by cutting them with a metal sheet. After curing, the uneven surface of the printed samples was cut to provide a uniform cover and an even surface for chloride exposure. Others chose to core cylindrical specimens out of larger prints. Moelich et al. [85] printed multilayered specimens and saw-cut 70 mm diameter concrete disc samples 21 days after printing in the out-of-printing-plane direction, resulting in 40 mm thick discs (i.e., equal to the layer thickness). The discs were subsequently saw-cut for the second time in order to remove bulging on one side and obtain a flat surface, resulting in 30 mm thick discs for chloride testing. Surehali et al. [86] printed multiple elements of size $200 \times 200 \times 200$ mm^3 having different layer heights (6, 13, and 20 mm), and, after curing for 28 days, extracted cores (100 mm diameter, 200 mm thickness) in all three orthogonal directions (see Fig. 9) for the three different layer heights. Subsequently, the cores were sliced into smaller discs of 50 mm thickness.

Another important aspect to be considered is the testing procedure. Chloride tests can, in general, be divided into two groups: natural (i.e., diffusion-based) and accelerated (using a potential difference). Both approaches have been used on printed concrete. Van Der Putten et al. [34] subjected their specimens to diffusion by immersion in a 3 % NaCl solution for up to 70 days. To ensure unidirectional chloride diffusion, all specimen sides except for the exposed surface were coated with epoxy. Malan et al. [57] exposed their specimens to ponding cycles of two weeks with a 5 % NaCl solution to simulate very severe chloride conditions in the marine tidal and splash zones. Bran-Anleu et al. [59] exposed their specimens to chlorides by means of capillary rise for 24 h, with the exposure solution consisting of 1 M NaCl + 0.1 M NaOH + sat. $Ca(OH)_2$. On the other hand, accelerated tests have been used by Moelich et al. [85] who used a chloride conductivity index in which a potential difference is applied across the sample to accelerate the movement of chlorides. Surehali et al. [86] followed the non-steady state migration procedure prescribed by NT Build 492 [87]. A major advantage of these accelerated tests is that results can be obtained in 1–2 days, making them more suitable for practical applications.

Care must be given to the interpretation of the chloride ingress results. Typically, for conventional cast concrete, a diffusion coefficient that can provide information about the chloride transport can be computed from the above-mentioned diffusion and migration tests. The diffusion coefficient is used for the service life estimation calculations. However, due to the heterogeneities and anisotropic nature of the 3D printed elements, this approach may not be suitable. Surehali et al. [86] investigated the effect of transport directions and layer dimensions on the non-steady state chloride migration coefficient and reported the significant directional dependency in the diffusion coefficient.

3.1.5. Freeze-thaw resistance

Freeze-thaw (FT) is an important durability issue that determines the service life of concrete structures in cold regions. A handful of studies examined the FT resistance of 3D printed concrete [15,26,48,88–92]. Typically, in these studies, FT damage is quantified by measuring the mass loss, strength loss, or dynamic modulus of elasticity with progressing FT cycles. FT tests can be done as freezing and thawing in water, freezing in air, and thawing in water [34,93]. According to the available

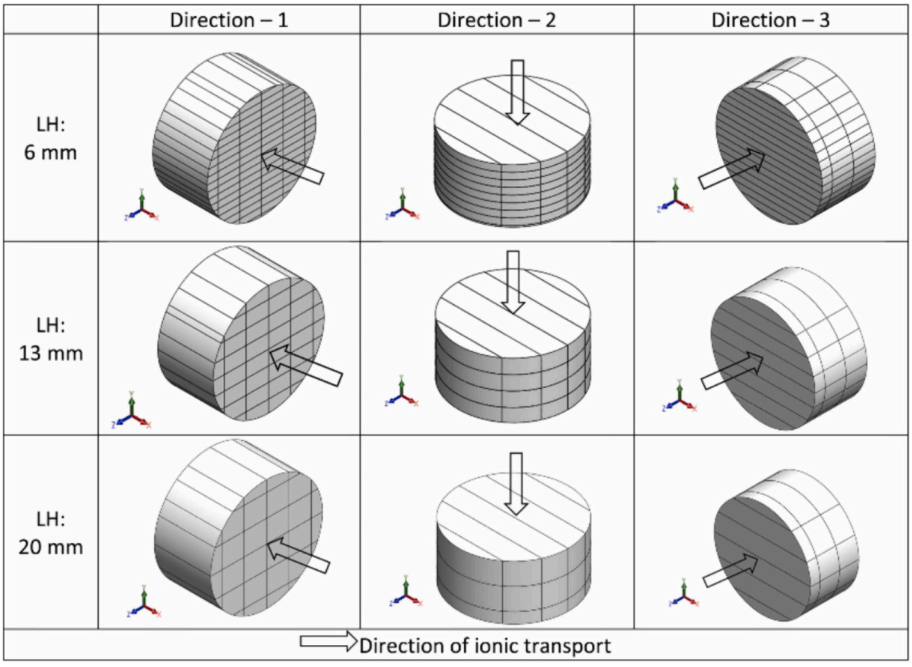


Fig. 9. Schematic illustration of ionic transport pathways in three orthogonal directions for specimens printed with different layer heights. The lighter shade represents the layers, while the darker shade indicates the interlayer region (taken from [86]).

literature, further effort is required to find a better freeze-thaw method and understand the deterioration mechanisms of 3DPC materials caused by cyclic freezing and thawing.

Salt scaling is another durability issue of concrete, defined as superficial damage caused by the freezing of a saline solution on the surface of a concrete body [94]. The damage is progressive and consists of the removal of small chips or flakes of material. Recently, Mohan et al. [9,25] assessed the resistance of 3D printed concrete against salt scaling. The authors drilled 50 mm Ø and 40 mm thick disc specimens from 3D printed wall elements and carried out the salt scaling tests according to CEN 12390-9 [95].

3.1.6. Sulfate and (sulfuric) acid attack

The extent of concrete degradation during sulfate and (sulfuric) acid attack depends on the concrete porosity and solution concentration. These tests are critical to assess 3D printed concrete's durability, providing insights into its application suitability. Recently, Rui et al. [96] measured the resistance of 3D printed elements against sulfate attack up to 150 wet-dry cycles. The study involved a wet cycle with submerging in a solution of Na_2SO_4 at a concentration of 5 % for 15 h and a dry cycle for 0.5 h. In a study by Baz et al. [97], sulfuric acid attack tests were conducted on both 3D printed and mold-cast mortar samples made of three different mix designs. The test procedure was adopted from ASTM C1012 [8]. Zhang et al. [26] conducted up to 150 times dry-wet cycling sulfuric acid attack in a 5 % Na_2SO_4 solution, guided by Chinese National Standard GB/T 50082 [98].

3.1.7. Abrasion

Limited literature is available regarding the abrasion resistance of 3DPC and, therefore, existing standard test methods for conventional concrete/mortar, such as the ASTM C944 [100] for concrete and mortar surfaces or the ASTM C779 [99] for horizontal concrete surfaces [113,114] can serve as a starting point. Similar test methods could be referred to in BS EN 13892-3 and BS EN 13892-4 [100,101]. With proper surface treatment, i.e., surface flatting or grinding after the printing process, the aforementioned methods could still be adopted to the 3DPC specimens for abrasive tests.

3.1.8. Shrinkage

Drying-induced shrinkage and the resulting cracking are other major durability problem for cement-based materials if the element has a high surface area to volume ratio, lack of formwork protection, exposure to extreme drying conditions, etc. As 3DPC is exposed to environmental drying (sometimes very harsh), drying shrinkage could be significantly higher compared to conventional cast concrete. In addition, the lack of coarse aggregates and high binder content exacerbates the problem [10,11].

Currently, there are very few methods to measure the early shrinkage of 3DPC as shrinkage assessment is, in general, a challenging task. In a recent review, early-age shrinkage measurement techniques that are especially suitable for 3DPC are summarized [102]. Broadly, the measurement techniques can be classified into contact-based (sensor embedded in the matrix or using LVDTs) and non-contact-based (digital image correlation (DIC) and laser displacement method) techniques [102]. Out of these methods, DIC is the most promising technique for shrinkage assessment. DIC offers advantages, including speed, accuracy, non-contact nature, relatively high cost-effectiveness, and, most importantly, the ability to provide complete surface displacement data, which is crucial for 3D printable concrete where significant variations in the spatial distribution of shrinkage strain can occur. Because of these advantages, DIC gained huge attention to assess the shrinkage of 3D printed elements. Moelich et al. [103] assessed both free and restrained shrinkage of 3D printed elements exposed to a moderate rate of evaporation using DIC. Their DIC measurements employed two different targets: one was a marker embedded within the specimen (see Fig. 10a), while the other involved the application of white and black chalk-based spray paint on the specimen's surface (see Fig. 10b). In addition, due to their layer-wise fabrication method, the regions between the layers may exhibit different shrinkage behaviour compared to the bulk regions of the material. Since DIC can provide full-field surface deformation, it can elucidate how the distribution of shrinkage strain varies spatially in 3DPC elements. Moelich et al. [85] evaluated the shrinkage behaviour of a 3DPC wall element with steel rods fixed at the base and inserted through the specimen. As the rods were anchored at the base, the DIC analysis revealed a linear increase in shrinkage strain from the bottom to the top of the specimen. However, a reduction or dip in shrinkage strain was noted at the interlayer regions as the strain transitioned from one layer to another. The authors attributed this to an interlayer slip occurring within the 3DPC element. Such shrinkage-related effects can lead to debonding or a decrease in the strength of the bond between layers, ultimately compromising the strength and durability of 3DPC elements [85,103–105]. In addition, inserting the rods to induce the restraining effect could result in microcracks in the matrix, especially in rapidly stiffening bi-component systems. On the other hand, these rods could simulate lintels in 3DPC houses, which will have the same restraining effect.

However, there are several challenges associated with using DIC and accurately obtaining the shrinkage data. One major challenge is associated with the speckle pattern utilized in DIC measurements. Using the most suitable speckle (spray, powder, etc.), changes in evaporation rate due to the surface coverage by the speckles, absorption of the speckled material to the sample, mixing of the speckled material with surface bleed water, etc., could potentially result in experimental artefacts or inaccurate results in the DIC analysis. Maintaining consistent and non-fluctuating lighting is crucial for DIC measurements. This becomes particularly challenging in early-age shrinkage studies; as fresh concrete begins to harden, it undergoes a colour change that can alter the brightness level of the speckle pattern. Though DIC offers a versatile and

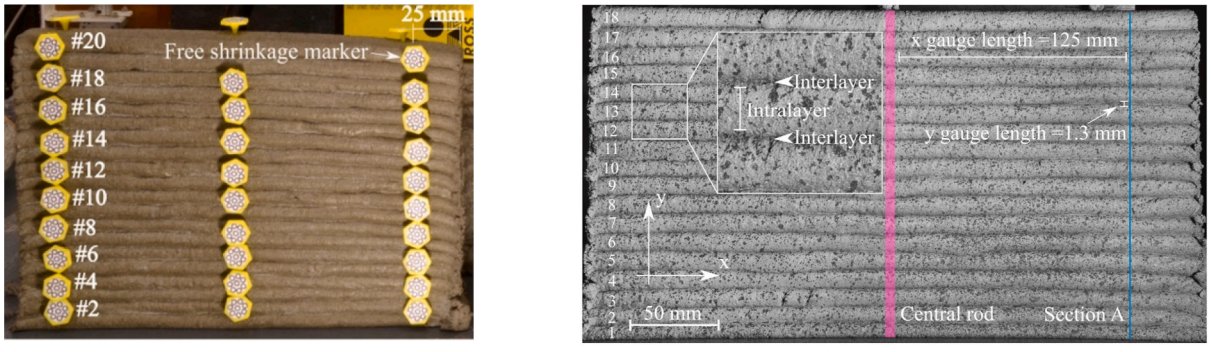


Fig. 10. Early-age shrinkage assessment in 3D printed wall element using (a) embedded markers and (b) chalk paint-based speckle pattern (taken from [103]).

powerful tool for early-age shrinkage assessment, further investigation is necessary to address the aforementioned challenges [102].

There are some recent studies focusing on using distributed fibre sensors to assess the shrinkage of 3D printable mixtures. Between each printed layer, a fibre sensor was longitudinally placed and shrinkage strain was continuously monitored [106,107]. The authors compared the accuracy of this technique with a DIC system and reported that the accuracy is comparable. Though the technique seems promising, the major drawbacks include slippage, interlayer debonding, shrinkage assessment restricted only to the interlayer region, lack of intralayer shrinkage assessment, impairment of geometric freedom, and low economic feasibility.

3.1.9. Exposure to fire and elevated temperature

Concrete generally possesses low thermal conductivity and non-combustible characteristics, resulting in good fire resistance [108]. By specifying adequate concrete cover, steel reinforcement can be protected against strength loss associated with elevated temperatures. This holds mostly for normal-strength concrete; high-strength concrete (defined as concrete with a cylinder compressive strength of 60 MPa or more at 28-day curing age [109]) typically comprises of smaller free pore volume resulting from a denser micro-structure, making it more susceptible to thermo-hygral spalling. In such cases, pores are filled with high-pressure water vapor more rapidly at elevated temperatures with slow diffusion of these molecules through the concrete due to its lower porosity. The result is explosive spalling of concrete. Some 3D printed concrete materials possess high compressive strength (often >60 MPa) [111] due to their low water-to-cement mass ratio and high cement content. Cicione et al. [49] investigated the fire behaviour of high-strength 3DPC at elevated temperatures using radiant panels and compared the results to that of cast samples of the same mix composition.

3.1.10. Other durability issues

Alkali silica reaction (ASR) is a major durability issue associated with concrete elements. It is a chemical process involving a reaction between reactive components (silica forms) in aggregates and the alkali (K^+ and Na^+) and hydroxyl (OH^-) ions found in the concrete's pore solution. However, it has not yet been investigated in the context of concrete 3D printing [110,111]. Though there is plenty of literature focusing on the tests to accurately assess ASR, the ideal test method should quickly and accurately evaluate the potential for ASR expansion in specific material combinations. It must reliably predict field performance, use the actual reactive aggregate(s) in question, and avoid excessive aggregate processing, such as crushing coarse aggregate for mortar testing. The methods should assess the impact of cement alkalis without artificially increasing alkali levels and deliver results within weeks or months, not years. Additionally, it should be able to evaluate all types of SCMs, lithium compounds, and their combinations with cement of varying alkali content [111]. In addition, the test methods have to be adapted to capture the printing process-related parameters, and therefore, in-depth studies are needed in this direction.

Another issue that needs attention in 3D printed concrete is long-term creep, as it can cause deformations and cracks and, thereby, durability issues. To understand why a concrete element cracks after prolonged exposure to the environment, we must consider how concrete responds to sustained stress or strain. The phenomenon where strain gradually increases over time under a constant level of sustained stress is known as creep. Depending on the degree of restraint, there can be cracking in the printed elements due to the creep. Currently, there are no studies that focus on the long-term creep behaviour of 3D printed concrete elements. The 3DPC may behave differently from the cast concrete due to the presence of interlayer regions and resulting anisotropy.

3.2. Findings related to the durability-specific applications of 3D printed elements

Based on gravimetrical measurements of capillary water sorption tests, Van Der Putten [77] demonstrated that longer time gaps between layers result in a decrease in the initial rate of water sorption. This finding is in line with expectations, as it was shown from a CT analysis of the interlayer zone that larger time gaps result in larger pores at the position of the interlayer. Knowing that the capillary action is inversely related to the pore radius, it is logical that, for these larger pore sizes, the initial capillary action decreases until gravity is overcome. The secondary absorption rate increased for samples with larger time gaps as, from that moment in time onwards, diffusion became more important.

Although the oxygen permeability test has not yet been used frequently to investigate the transport properties of 3DPC, the study of Van Steenkiste and Wauters [77] showed that this test method could be useful in assessing the durability of 3DPC. For printable mix compositions with a higher w/c, higher permeability levels were obtained as expected. In addition, the effect of different layer thicknesses and different storage conditions was investigated. It was shown that increasing the layer thickness reduced the measured permeability, which is logical as the number of interlayers decreases. Curing the printed samples at 95 % instead of 60 % relative humidity resulted in a >50 % decrease in permeability, which shows that this test also correctly reflects the effect of the storage conditions and, thus, the effect of (drying) shrinkage on the durability. Drying of the samples was performed at both 40 °C and 60 °C (for both temperatures, samples remained in the oven until the mass loss became smaller than 0,1 % in 24 h). As it was shown that samples dried at 60 °C had a >90 % lower oxygen permeability, it was concluded that the increased drying temperature resulted in a change in micro-structure, and it was therefore suggested to include a drying procedure of 40 °C when performing this test. For some of the layered wall elements in the study of Van Steenkiste and Wauters [77], a time gap of 10 min was foreseen before printing the next layer, including a few cold joints. Also, this effect was demonstrated in the outcome of the oxygen permeability test as a 30 % increase in permeability was noticed for drilled concrete samples, which also included a cold joint. In the study of Van Steenkiste and Wauters [77], printed samples with a diameter of 50 mm were surrounded by an impermeable coated concrete ring to avoid any oxygen ingress from the sides of the samples. To increase the exposure surface, these authors also investigated the possibility of making use of 100 mm diameter test samples. For the latter samples, a higher permeability was measured compared to the 50 mm diameter samples as a result of the increased number of interlayers.

A thought that could be made when preparing the samples for the oxygen permeability test, but in extension also for all other durability tests, is that when samples are drilled from linear wall elements at different heights within the elements, this could result in large variations in the test results as the properties of the interlayers might differ for different heights within the element due to the higher compaction of the lower layers.

Interlayer regions forming weak zones causing preferential ingress of aggressive agents is also clear from the micro XRF chlorine map shown in Fig. 11 obtained for a 3DPC sample exposed to a chloride solution. It can be seen that chloride penetration happened from the bottom surface and the interlayers (indicated with dashed lines). The preferential transport of chloride ions through the interlayer region could clearly be noticed.

Das et al. [91] assessed the FT resistance of both printed and cast specimens using ASTM C666 [93] and observed that the 3D printed specimens displayed lower FT resistance in comparison to cast specimens due to the presence of high capillary porosity at the interface between the printed filaments. Assaad et al. [90] reported that the interfaces between layers are more susceptible to damage from FT cycles compared to the bulk of the 3D printed mortar filaments. They noted

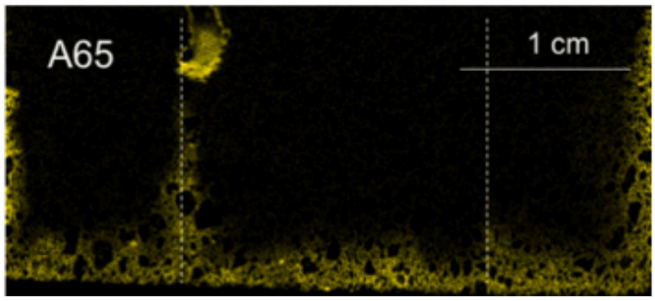


Fig. 11. Micro XRF chlorine map for sample exposed to chloride solution. Chloride penetration happened from the bottom surface and the interlayers indicated by dashed lines. Yellow colour indicates chloride ions and the intensity of the colour is proportional to the quantity of chloride ions (taken from [59]). (For interpretation of the references to colour in this figure legend, the reader is referred to the web version of this article.)

that there was a more significant reduction in the interlayer bond strength (two to three times) compared to a decrease in compressive and flexural strengths when subjected to FT cycles. Zhang et al. [26] observed more significant FT damage in printed specimens compared to cast samples using dynamic elastic modulus measurements. The authors concluded that FT-induced damage primarily occurred along weak printed interlayers and that aggregates were more challenging to dislodge from the surface of printed specimens than from cast samples due to the extrusion pressure, which led to a densely packed surface in the printed materials. Van der Putten et al. [34] reported that the prolonged interlayer time gap has an insignificant effect on the FT performance. Ghantous et al. [89] assessed the influence of the printing directionality on the FT performance of the 3D printed elements. The authors correlated the FT performance of elements made with various degrees of saturation using thermomechanical analysis and compared it with cast specimens. The decrease in mechanical performance for the 3D printed specimen was lower than for the cast specimen after FT cycles. The authors observed that 3DPC has a much higher resistance to salt scaling compared to mold-cast concrete. The higher resistance against salt-scaling damage could be due to the suction created from the ice formation in the interlayers of printed concrete, thereby compensating the glue spall stress from the ice formation on the surface concrete. Authors also observed that the volume of pores at a size range of 100–0.1 μm reduces nearby interfaces, which could indicate that the interfaces can act as air voids present in the system [9,25].

Related to acid attack, Zhang et al. [26] asserted that 3DPC exhibits higher resistance to sulfuric acid attack compared to conventional cast concrete. The results were further confirmed by Rui et al. [96], in which 3DPC reaches the maximum grade in sulfuric acid resistance according to the Chinese standard [98]. It should be highlighted that the anisotropy of 3DPC was only reported when large voids and pores were continuously present at the interlayers [96], which is highly related to the printing quality, i.e., the mix design and printing parameters of the 3D printed concrete.

Another durability issue associated with the 3D printed concrete elements is the expansion and cracking due to sulfate attack. Tin, the 3D printed concrete systems made with in-line accelerator injection (2 K systems) generally utilize the alkali aluminium sulfate. When the aluminium sulfate remains unmixed in the concrete, it can result in delayed ettringite formation, promoting an internal form of degradation. The influencing factors include the content of aluminium and sulfate in the alkali-free admixtures, the presence of sulfate-rich components in the mixtures, the type of cement used, the dosage, and the sulfate content in the clinkers [112,113]. Therefore, it is crucial to assess the extent to which internal sulfate attacks 3D printed concrete systems that use aluminium sulfate as an accelerator [114].

When it comes to drying shrinkage, there are significant differences between 3DPC and cast concrete. Moelich et al. [103] reported significant free shrinkage occurring within the first 2 h being strikingly higher than in conventional concrete. Furthermore, when the shrinkage was constrained, the 3DPC elements cracked at a very early age. One of the major applications of 3D printed concrete is its use of stay-in-place formwork filled with infill concrete. In such applications, shrinkage compatibility between the 3D printed formwork and the infill concrete is very important. Differential shrinkage could lead to debonding failure, which can significantly reduce the safety and durability of the entire structure [115]. In addition to the differential shrinkage, moisture warping and thermal curling could also influence the performance of the 3D printed stay-in-place formwork [116].

Regarding the performance at elevated temperatures, in a recent study, Cicione et al. [49] reported that the cast samples all experienced thermo-hygral spalling, as would be expected of high-strength concrete, though the 3D printed samples did not experience any spalling. Instead, the printed samples delaminated at the weak interfaces, indicating no residual strength post-fire conditions. The authors attribute this finding to the interconnected voids at interfaces, resulting not only in higher permeability for high-pressure water vapor to escape but also weaker filament bonding that cannot resist thermal gradient-induced self-equilibrating tensile stresses. This finding was corroborated by Dong et al. [117] and Arunothayan and Sanjayan [118] for ultra-high performance 3D printable concrete (compressive strength exceeding 150 MPa). Xiao et al. [119] executed experimental research on the mechanical properties of 3D printed recycled mortar after high-temperature exposure. The results revealed that the degradation pattern of mechanical properties in 3D printed recycled mortar after high temperatures mirrored that of trial mold castings, with high temperatures displaying a stratified influence on the central interface of 3D printed recycled mortar layers (Fig. 12). Considering that most realized 3D printed structures are thin-walled (optimized geometries using less material than cast counterparts), the non-spalling behaviour at elevated temperatures observed in literature is especially welcome. However, preliminary research simulations at the structural level indicate that wider filament layers and wall sections for 3D printed concrete structures are required to obtain adequate fire performance [120,121].

Cracking of the matrix due to the early age thermal expansion is another critical issue for 3D printed concrete structures. This is even more critical in two-component (2 K) systems due to the very fast hydration reaction and associated heat release. As the hydration reaction is accelerated, the printed structures gain strength and form a rigid microstructure, which can crack due to the thermal expansion. Currently, there is seldom literature available that focuses on the early-age thermal cracking of 3D-printed concrete structures manufactured

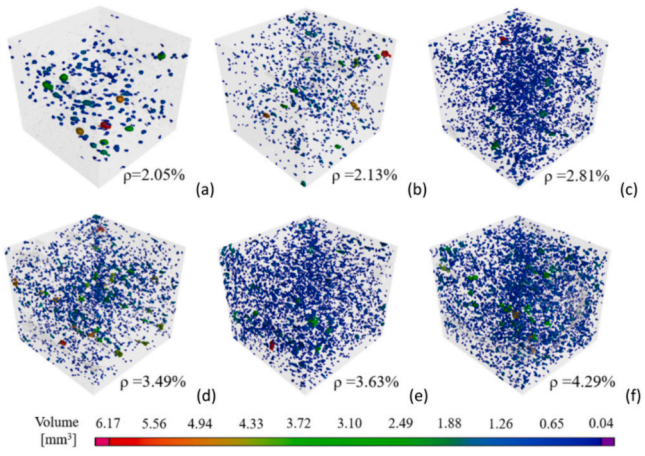


Fig. 12. Porosity visualization of 3DPC after exposed to (a) room temperature, (b) 200 °C, (c) 400 °C, (d) 600 °C, (e) 800 °C, and (f) 1000 °C [taken from [122]].

using the 2 K method [114].

4. Attempts to improve the micro- and meso-structure and durability of printed elements

It is clear from the previous sections that 3DPC presents numerous durability concerns mostly originating from their altered micro- and meso-structure. Compared to cast concrete, 3DPC requires certain *material, process* and *geometrical* amendments, resulting in a less favourable micro- and meso-structure as an unintended consequence. Considering that no guidance, whether prescriptive- or performance-based, is currently available to ensure sufficient durability of 3DPC structures, many researchers undertook to devise solutions to specific durability concerns that are noted in the literature. This section elaborates on these solutions and their efficacy, and we distinguish between i) bulk material (*material-related*), ii) interlayer regions (*process-related*), and iii) indirect solutions toward improving 3DPC durability. Table 1 presents a summary of all these solutions and their efficacy.

4.1. Bulk material

It is well documented that 3DPC typically contains smaller-sized aggregates, higher powder contents, and more chemical admixtures (e.g. accelerators) that collectively increase the risk for shrinkage cracking compared to conventionally cast concrete. Cracking that arises from plastic, drying or autogenous shrinkage enhances durability issues, creating pathways through which deleterious substances can be transported. This is linked to two primary aspects: i) the 3DPC material is inherently more prone to shrinkage, and ii) minimal and/or ineffective curing measures are currently employed for 3DPC structures. A study by Moelich et al. [123] investigated multiple plastic shrinkage and cracking mitigating measures, including self-releasing superabsorbent polymers (SAPs), retentive SAPs, a shrinkage-reducing admixture (wax emulsion), external water application both one-time and in 20-minute intervals, calcium aluminate (CA) and calcium sulfoaluminate (CSA) cements as partial replacement of Portland cement (PC), and 6 mm polypropylene microfibre addition at 0.3 % by volume. Sorptivity kinetics dictate SAP classification, where self-releasing SAP refers to the continuous release of water, while retentive SAPs only release water due to an external trigger such as internal humidity drop or capillary suction. The results

Table 1
Summary of mitigating measures employed in literature to improve micro- and meso-structure of 3DPC toward enhanced durability.

Classification	Mitigating measure	Brief description	Efficacy	Reference to study
Bulk material	Superabsorbent Polymers	Self-Releasing	Low	Moelich et al. [123]
	Superabsorbent Polymers	Retentive	Low	
	Shrinkage Reducing Admixture	Wax Emulsion	Low	
	Multiple Water Application	20-minute interval external water application	Medium	
	Single Water Application	One application of externally applied water	Low-to-Medium	
	Calcium Aluminate Cement	Rapid setting cement at 8 % replacement of PC	High	
	Calcium Sulfoaluminate Cement	Rapid setting cement at 8 % replacement of PC	High	
	Fibre	6 mm Polypropylene fibre at 0.3 % volume	Very High	
	Superabsorbent Polymers	Multiple different polymers used in the study	Very High	Van der Putten et al. [124]
	Clay Mineral	Replacement of PC with Attapulgite by up to 3 %	Low	Yao et al. [125]
	Processing Parameters[a]	Synergy between pumping, extrusion and acceleration of mix setting time	Low-to-High	Das et al. [91]
Interlayer region	Cement Powder[a]	0.16 g/cm^2 dosage	Low	Van der Putten et al. [129]
	Combing[a]	34 needles with a 1 mm diameter	Medium	
	Sand Particles[a]	Maximum 2 mm particle size	Medium	
	Water[a]	Moisturization of filament surface	Low	
	Print speed[a]	Slower print speed employed	High	Van der Putten et al. [129]
	Thermo-hydrokinetics[a]	Steaming of the interlayer just before placement of the overlay	High	Munemo et al. [130]
	Mortar Bonding Layers[a]	Multiple types of chemistries	Very High	Ma et al. [132], Marchment et al. [133], Wang et al. [134] & Hosseini et al. [135]
	Topological Interlocking[a]	Various interlayer geometries imparted onto the filament surface	High	Mostert & Kruger [137]
	Sealing or Covering[a]	Plastic film or wet blanket	High	Chen et al. [35]
	Strengthening Agent[a]	Bi-component strengthening agent consisting of calcium and silicate	High	Geng et al. [131]
	Water[a]	Increase surface moisture content	Low	Weng et al. [141]
	Cement Paste[a]	0.26 w/c ratio PC cement paste	Low	
	Polymer Solution[a]	1:4 ETONIS LL5999-8331 polymer powder-to-water mass ratio	Medium	
	Cement Strengthener[a]	Commercialized W1 Cement Strengthener	Medium-to-High	
	Cement Paste	0.35 w/b ratio PC cement paste	Medium	Mohan et al. [136]
	Latex Addition	Styrene butadiene rubber (SBR) at 15 % of binder mass	Medium	Assaad, Hamzeh & Hamad [90]
Indirect	Enclosure on Site	Full, partial, or roof only	Low-to-Very High Depending on Conditions	Moelich et al. [104] & Keita et al. [36]
	3D Printed Stay-in-place Formwork	Permanent 3D printed concrete formwork providing cover for inner cast concrete	Low-to-Very High Depending on Stay-in-place Formwork Thickness	Bekaert et al. [17] & Sanchez et al. [58]

[a] These studies have not directly assessed the mitigating measures' influence on a durability mechanism; however, the authors believe the mitigating measures possess potential to achieve the indicated efficacy levels.

indicate fibers to be the overall best solution, both yielding the largest reduction in free plastic shrinkage (almost 50 % less than the reference mix) and mitigating any cracking from occurring. Following this, the CA and CSA cements performed second best at only 8 % substitution of PC, though it did not prevent cracks from forming. Surprisingly, the 20-minute interval water curing performed very similarly to the CA and CSA cements, while the remaining mitigation measures were largely ineffective. Fig. 13 depicts the performance of these mitigation measures. In contrast to this, a study by Van Der Putten et al. [124] also investigated the use of SAPs on plastic shrinkage and found them to mitigate shrinkage by up to 200 %. Additionally, they decreased the number of nanopores and increased the number of pores above 700 nm, resulting in less permeability (or microcracks) that act as ingress paths for chemical substances. Yao et al. [125] included Attapulgite, a clay mineral, into a PC mortar with up to 3 % replacement of mass. It was found that the carbonation depth, as well as the chloride ion depth at the interface, increased dramatically as the percentage of Attapulgite inclusion increased. Hence, early research suggests Attapulgite inclusion to be detrimental to the durability performance of 3DPC.

4.2. Interlayer regions

The interlayer regions in 3DPC structures typically comprise higher porosity and permeability that, in essence, act as microcracks through which chemical substances can travel [123]. Additionally, it is also the cause of weak bonding between layers [41]. Generally, the time gap (time between the deposition of two subsequent layers) governs the degree of bonding since the evaporation of moisture at the layer surface is one of the main mechanisms responsible for premature debonding [126]. However, the evaporation rate from climate conditions at the printer location, together with the rate of hydration of the printable material, must be considered together with the time gap [127]. Ideally, the time gap must first be optimized by using optimal print parameters (i.e., reduced as much as possible while avoiding structural failure in the fresh state) [128] before opting for other mitigating measures.

Van Der Putten et al. [129] investigated multiple measures to improve interlayer bonding strength in 3DPC, which is coupled to the microstructural density of those regions. The authors i) added cement powder between layers at 0.16 g/cm^2 dosage, ii) used a comb with 34 small needles to roughen the surface, iii) added sand particles of 2 mm maximum size between layers and iv) added water (moisturization) on the layer surface just before deposition of the following layer. The sand had the most notable influence on surface roughness, followed by the comb. The addition of water reduced the surface roughness. All measures reduced the interlayer bond strength tested at a 0 min time gap, except the comb measure, which yielded a 21 % improvement. About a 48 % decrease in bonding strength was observed between the 0 and 30-minute time gap specimens, while no measure could improve the bonding strength of the reference specimen tested at a 30-minute time gap. In another study by the authors [66], they investigated the effect of the print speed on the surface roughness, interlayer bonding strength, and porosity. The results indicated that slower print speeds yield higher layer surface roughness (more than double the surface roughness at 1.7 vs 3 cm/s print speed). The effects hereof are evident in the mechanical testing, where the slower print speed consistently yielded higher interlayer bonding strengths for various time gap intervals. MIP results showed that the open (capillary) porosity for lower print speeds is higher; however, the pores at higher print speeds are significantly larger, thereby indicating potentially poorer durability performance of 3DPC when printing at higher speeds. Munemo et al. [130] developed a thermo-hydrokinetics application to improve interlayer bonding between 3DPC layers. The method consists of steam applied on a substrate layer immediately before the overlay layer is placed. A 78 % increase in bonding strength was obtained for a steamed specimen compared to a reference specimen, tested at a 0 min time gap. All steamed specimens outperformed the reference samples at 7 and 28-day curing ages, as well as for 0, 5, and 10 min time gaps. SEM images further indicated a denser interlayer micro-structure with smaller voids for the steamed specimen compared to the reference specimen. Geng et al. [131] applied a bi-component interface strengthening agent to 3DPC interfaces. This consists of 10 wt% calcium formate solution for component A and 13.4 wt% lithium silicate, 3.6 wt% sodium silicate, 1.0 wt% nano-silica, and 0.2 wt % ethylene diamine tetra acetic disodium salt mixture for component B. This resulted in a 106 % increase in splitting tensile strength due to densification of the interface region. A further frequently encountered measure in literature is the application of a mortar bonding layer between 3DPC filaments. These bonding layers can comprise i) PC and CSA cement blends [132], ii) PC with chemical additives such as viscosity modifying additives [133], iii) high belite CSA cement containing epoxy resin or chloroprene latex-based polymers [134], and iv) synthesized polymer of sulfur (99 %) and black carbon (1 %) mixture with sand [135]. All these measures successfully improve interlayer bonding, with the most notable result emanating from the epoxy resin CSA mortar. Although not affecting the concrete micro-structure directly, these mortar bonding layers would result in a denser interlayer region, ultimately improving durability performance. Mohan et al. [136] added a thin layer of cement paste in between two subsequent layers to reduce the chloride ingress measured according to NT BUILD 492 [87]. The time gap was limited to 60 s. The addition of the cement past layer resulted in a significant reduction in steady-state chloride migration of

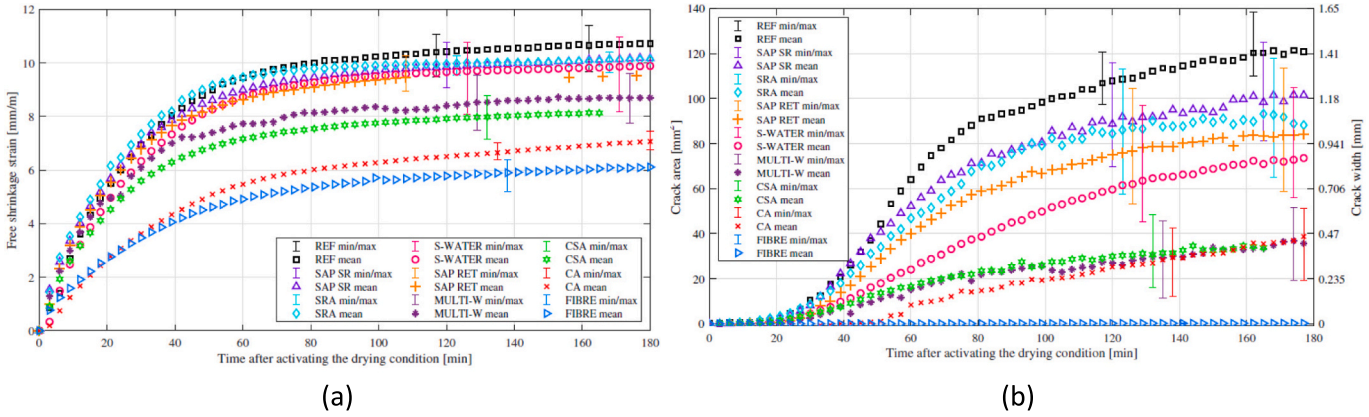


Fig. 13. Median free plastic shrinkage (n = 6) (a) and crack area/width (n = 4) (b) of 3DPC considering various mitigating measures. REF – reference, SAP RET – superabsorbent polymers retentive, SAP SR – superabsorbent polymers self-releasing, SRA – shrinkage reducing admixture, S-WATER – single external water application, MULTI-W – multiple external water applications in 20-minute intervals, CSA – calcium sulfoaluminate cement (at 8 % substitution of PC), CA – calcium aluminate cement (at 8 % substitution of PC), FIBRE – 6 mm polypropylene fibre (taken from [123]).

the printed concrete. Topological interlocking has also been found to improve interlayer bonding strength [137]. The typical horizontal interlayer is altered with the inclusion of inclined or vertical planes (e.g. through the inclusion of interlocking teeth). Although this is principally a mechanical and not chemical mechanism, it is postulated that the topologically altered interlayer path will prevent or hinder the ingress of chemical substances, thereby improving durability performance. Curing has also been found to be critical to the interlayer region's microstructure and strength. Chen et al. [35] recommended covering or sealing deposited layers with plastic film or a wet towel to improve bonding, especially in the case of long time gaps (up to 4 h), rather than keeping them exposed to ambient conditions.

4.3. Indirect solutions

It is well known that 3DPC structures are more prone to plastic shrinkage cracking as they are not covered by formwork like conventionally cast concrete, thereby being exposed to possible evaporation of pore water. Moelich et al. [104] have demonstrated that the magnitude of the evaporation rate has a considerable effect on plastic shrinkage and cracking risk in 3DPC. This has also been confirmed in a study by Keita et al. [36]. The evaporation rate is primarily linked to environmental conditions on site, including i) air temperature, ii) relative humidity, iii) wind speed, iv) exposure to direct sunlight, and v) concrete temperature. Note that the concrete temperature is primarily influenced by the cement type used and the hydration heat released from the exothermic reaction. Not only do high evaporation rates result in plastic shrinkage cracking of the bulk material, but also severely affect interlayer bonding that could collectively compromise durability performance. In a further study, Moelich et al. [127] found that for benign evaporation rates (similar to indoor conditions ~0.05 kg/m^2/h), the interlayer bonding strength reduces by 107 % when the time gap is increased from 1 to 30 min. When exposed to severe evaporation rates (similar to on-site conditions ~1 kg/m^2/h), the interlayer bond strength decreased by an additional 35 % at a 30-minute time gap. It is, therefore, critical to control the evaporation rate as far as is practically possible, in addition to employing curing methods. This can be achieved by constructing an enclosure around the object to be printed on-site. Depending on the enclosure details (e.g., complete, partial, or roof cover only, as shown in Fig. 14), environmental conditions can be controlled accordingly to yield a desired evaporation rate whereby the plastic shrinkage cracking risk is acceptable and likely to prevent durability issues from arising. 3D printed stay-in-place formwork, which remains permanently in place after inner cast concrete has hardened, is an alternative solution to large enclosures [17,58]. The printed formwork skin is exposed to environmental conditions, protecting the inner structural/load-bearing concrete therefrom and ensuring enhanced durability performance in both the fresh and hardened concrete states.

5. Challenges to be tackled and opportunities to implement 3DPC knowing the shortcomings related to their micro- and meso-structure and durability

3DPC is a promising new technology for the construction industry. The increased form freedom and the labour reduction are key aspects in promoting the technique. Despite the intensive research performed in the last decade, a large number of challenges remain. The largest one is ensuring and improving the durability of 3DPC structures. As mentioned in previous sections, 3DPC may have a significantly lower durability performance than traditional cast concrete. The lack of proper curing and the layer-wise build-up of printed concrete elements are the main reasons for this. Therefore, focusing on these aspects to improve the construction's durability performance should be key. Nevertheless, trying to improve these aspects comes with challenges to be overcome.

The lack of proper curing results from the absence of formwork. This results in high early shrinkage of the printed material, leading to (plastic) shrinkage cracks in the concrete element [85,103,123]. In the case of reinforced 3D printed structures, these shrinkage cracks increase the risk for reinforcement corrosion due to the facilitated ingress of aggressive substances such as CO_2 and chlorides, which can significantly reduce the elements' service life [142]. Additionally, the loss of water due to drying can lead to a reduction in concrete hydration and a less dense microstructure. Therefore, preventing evaporation of the mixing water within the printed concrete is needed. The most convenient way is to print within a controlled environment rather than onsite [85]. Within these controlled environments, environmental parameters can be properly monitored and even adjusted to create ideal circumstances. However, real challenges exist when 3D concrete printing has to be performed on-site. Environmental factors such as the location, time of the year, exposure to direct sunlight, relative humidity, and wind are never constant. Measurements have to be taken to prevent severe fluctuations and limit the influences of climatological circumstances. If not, high variations in material properties can be expected.

As also discussed in Section 4, several attempts have been made to better control the environmental conditions on-site. Immediately covering the structure with plastic sheets renders the best results but is not always feasible [143]. The placement of a tent or temporary structure around the printing space would be the next best option. Depending on the geological print location, the temporary structure prevents contact between the 3D printed structure and environmental conditions such as rain, sun, and wind. Additionally, it is possible to slightly adjust the conditions (temperature and humidity) within the temporary structure. Although this would be the best option on site, the placement of a temporary structure takes time and isn't without cost. At the same time, the solution is not always feasible, as the dimensions of the temporary structure will limit the size of the printed element.

As complete protection of the construction site is not always possible, internal and external curing methods have been proposed to improve the durability of on-site printed elements. As discussed in detail in Section 4, internal curing has been proposed through the addition of SAPs within the mixture [123,124]. The SAPs slowly release water over time and



(a) (b) (c)

Fig. 14. On-site control and/or mitigation of environmental conditions during printing via a) complete enclosure [138], b) partial enclosure [139] or c) roof cover only [140].

ensure proper curing. Although the method has shown effectiveness, some concerns exist, as introducing SAPs will alter the rheological properties of the printed mixture [123]. Another option is to use an external curing method. One option is to spray water on the outside of the printed elements. This curing technique creates an excess water film (similar to bleeding water) on the surface of the printed material which can evaporate instead of the mixing water. Although the latter proposed solution has shown effectiveness, the protection barrier is only temporary, and the application is not always feasible. Another option is the use of a curing agent (CA). The CA creates a vapor-slowing barrier on the element, that limits the evaporation rate. The benefit is that this method does not alter the concrete properties during printing, reduces the risk of plastic shrinkage cracks, and could easily be applied [85]. Nevertheless, the effectiveness of the CAs on the durability performance of 3D printed structures has not been shown yet. The problem with external curing is the way of properly applying the curing agent. Scaffolds and aerial platforms are needed but are not always allowed to reach or enter narrow spaces on the construction site. A mountable spraying system near the nozzle could offer relief. Despite the curing problem of 3D printed concrete being known, no standardization or guidelines exist for the current industry. A basic approach to limit evaporation and obtain proper concrete curing should be available to ensure the durability and performance of all printed structures.

Another challenge that has to be tackled to improve the durability is the influence of interlayers. An increasing time gap between the printing of two subsequent layers will lead to preferential ingress paths for aggressive substances. These preferential paths act like cracks and can significantly reduce the service life of a printed structure. Therefore, the performance of 3D printed elements is highly dependent on the performance of the interlayers. The challenge concerning durability exists to improve the interlayer in such a way that 3DPC can be seen as an isotropic material. One of the easiest methods to apply is to reduce the time gap between two printed layers [34]. Reducing the time gap between the layers can even be done for on-site 3D printing through optimization of layer height and print speed - the combination of which will determine the vertical building height. A suitable model can be used to optimize these print parameters while preventing failure during printing (i.e., printing too fast vertically) [128]. At that point, the interlayer shows a similar resistance against carbonation and chloride ingress as the bulk material. This means that during the design of a printing path, the length should be as short as possible to limit the time gap. However, for large construction sites, this is not feasible. In these situations, new methodologies are needed to improve and ensure a low porosity of the interlayer, such as applying cement paste between the printed layers [9] or delaying the hydration reaction of a previous layer until the next layer has been deposited. Not only the production methods have to be adapted but also the testing and design methods. Currently, only standardized methods are available for homogeneous cast concrete. In Section 3, it was already indicated that the interlayers influence the durability aspects of the printed material. As no specific guidelines exist to test the durability of 3D printed material, standardized tests have been widely adapted to the needs of each researcher individually. However, unified testing methods for the durability of 3D printed concrete are needed to assess quality control and standardization of the printing method properly. To a larger extent, standardized testing methods would open the way to proper design methods and service life estimation.

Despite the challenges existing within 3DPC, some opportunities also result from this placing method. The high degree of freedom during placement makes it possible to create complex and customized structures such as bridge beams, street furniture or reef elements, which today require expensive formwork. In future, 3DPC could also be used for fire protection casings of steel elements. The dense pore structure of traditional concrete makes it prone to spalling; however, when using 3DPC, the often higher porosity decreases the heat conductivity, which could improve fire protection [49]. Additionally, the high permeability results in a lower chance of spalling of the casing due to high vapor pressure.

Another opportunity would be to use printed concrete as a specifically designed concrete cover. Printed material could be designed specifically for a certain aggressive environment (high sulfate resistance, chloride resistance), while the infill material could be of a lower quality. At that point, the printed cover will protect the rebars and infill concrete. As a result, the infill concrete should not fulfill the environmental requirements. This means that concrete with lower quality or lower binder content could be implemented, which was previously not possible.

6. Conclusions

Most experts agree on the potential of 3D concrete printing technologies in improving construction productivity and workers safety along with contributing to a more sustainable construction industry through material use optimization. Their exact mode of application, their integration into our usual building processes or even the products market where they can potentially make a difference are, however, still to be defined.

Predicting the future of any disruptive new technology is always difficult but 3D concrete printing technologies encompass various families of shaping strategies applied to various cement-based materials. Over the last two decades, through experimental studies, analytical models, numerical simulations, and demonstrators, academic and industrial developments have challenged the strengths and limits of all these potential technologies for two main obvious reasons. On one hand, it has allowed for the improvement of these technologies and the development of the scientific and technical knowledge and skills required for their use and integration. On the other hand, the study of these strengths and limits progressively allows for the identification of the kind of objects they could reasonably help us produce.

The above efforts were mainly focused on the fresh properties of printable materials allowing for the process to shape a concrete element successfully. This was natural and expectable as these features were the main ones to be modified by such technologies. In parallel, as these technologies allow for increased freedom in structural design, the mechanical properties of this potentially anisotropic material were studied along with various reinforcement strategies.

This paper has focused on recent efforts, developments, and publications that tackle the last set of properties that will allow for the definition of the exact use of such printing technologies, namely the durability of printed concrete. This set of properties is expected, in turn, to drive the service life of printed parts and components. Results and methods extracted from almost 145 publications were presented, streamlined and discussed by 14 authors under the leadership of Prof. Kim Van Tittelboom. This resulted in this state-of-the-art paper covering the specifics of printed concrete durability, starting from the material microstructure and its assessment all the way up to some advanced solutions for durability improvement.

The present authors hope that this paper will allow for a better definition of our current state of knowledge, of the still pending questions and of our existing research needs. They moreover hope that it will contribute to strengthening and gathering our community around the key issues identified during the writing process. They finally consider that the question of the durability of printed concretes at the heart of this paper incarnates the last step needed to integrate these technologies in our standards and our industrial practices.

CRediT authorship contribution statement

Kim Van Tittelboom: Writing – review & editing, Writing – original draft, Visualization, Methodology, Investigation, Conceptualization. **Manu K. Mohan:** Writing – review & editing, Writing – original draft, Visualization, Methodology, Investigation, Conceptualization. **Branko**

Šavija: Writing – review & editing, Writing – original draft, Visualization, Methodology, Investigation, Conceptualization. **Emmanuel Keita:** Writing – review & editing, Writing – original draft, Visualization, Methodology, Investigation, Conceptualization. **Guowei Ma:** Writing – review & editing, Writing – original draft, Visualization, Methodology, Investigation, Conceptualization. **Hongjian Du:** Writing – review & editing, Writing – original draft, Visualization, Methodology, Investigation, Conceptualization. **Jacques Kruger:** Writing – review & editing, Writing – original draft, Visualization, Methodology, Investigation, Conceptualization. **Laura Caneda-Martinez:** Writing – review & editing, Writing – original draft, Visualization, Methodology, Investigation, Conceptualization. **Li Wang:** Writing – review & editing, Writing – original draft, Visualization, Methodology, Investigation, Conceptualization. **Michiel Bekaert:** Writing – review & editing, Writing – original draft, Visualization, Methodology, Investigation, Conceptualization. **Timothy Wangler:** Writing – review & editing, Writing – original draft, Visualization, Methodology, Investigation, Conceptualization. **Zhendi Wang:** Writing – review & editing, Writing – original draft, Visualization, Methodology, Investigation, Conceptualization. **Viktor Mechtcherine:** Writing – review & editing, Writing – original draft, Visualization, Methodology, Investigation, Conceptualization. **Nicolas Roussel:** Writing – review & editing, Writing – original draft, Visualization, Methodology, Investigation, Conceptualization.

Declaration of competing interest

The authors declare that they have no known competing financial interests or personal relationships that could have appeared to influence the work reported in this paper.

Data availability

No data was used for the research described in the article.

Acknowledgements

Dr. Manu K. Mohan acknowledge the financial support provided by the Industrial Research Fund of Ghent University towards the StarTT Twinmix project. Dr. L. Caneda-Martínez is supported by the “Post-doctoral fellowship funded by Xunta de Galicia (ED481B-2021-001). Dr. Michiel Bekaert acknowledges Buildwise for the financial support of his Ph.D. work. Dr. Timothy Wangler is fully or partially funded by the National Centre for Competence in Research – Digital Fabrication in Architecture (NCCR Digital Fabrication, Agreement # 51NF40-141853) from the Swiss National Science Foundation.

References

[1] American Concrete Institute, CT-18: ACI Concrete Terminology, Farmington Hills, www.concrete.org, 2018.
[2] CEN (European Committee for Standardization), EN 206: Concrete – Specification, Performance, Production and Conformity. www.nbn.be, 2013.
[3] CEN (European Committee for Standardization), Eurocode 2: Design of Concrete Structures - Part 1-1: General Rules and Rules for Buildings. www.nbn.be, 2015.
[4] fib (Fédération International du Béton), Fib Model Code for Service Life Design, 2006.
[5] D. Crete, General Guidelines for Durability Design and Redesign/Probabilistic Performance Based Durability Design of Concrete Structures - DuraCrete – Final Technical Report, Gouda, 2000.
[6] M.R. Geiker, M.A.N. Hendriks, B. Elsener, Durability-based design: the European perspective, Sustain. Resilient Infrastruct. 8 (2023) 169–184, https://doi.org/10.1080/23789689.2021.1951079.
[7] Y. Chen, Y. Zhang, B. Pang, Z. Liu, G. Liu, Extrusion-based 3D printing concrete with coarse aggregate: printability and direction-dependent mechanical performance, Constr. Build. Mater. 296 (2021) 123624, https://doi.org/10.1016/J.CONBUILDMAT.2021.123624.
[8] V. Mechtcherine, V.N. Nerella, F. Will, M. Näther, J. Otto, M. Krause, Large-scale digital concrete construction – CONPrint3D concept for on-site, monolithic 3D-printing, Autom. Constr. 107 (2019) 102933, https://doi.org/10.1016/j.autcon.2019.102933.
[9] M.K. Mohan, Towards Sustainable Concrete 3D Printing for Marine Structural Applications, Doctoral Thesis, Ghent University, 2023.
[10] M.K. Mohan, A.V. Rahul, G. De Schutter, K. Van Tittelboom, Extrusion-based concrete 3D printing from a material perspective: a state-of-the-art review, Cem. Concr. Compos. 115 (2021) 103855, https://doi.org/10.1016/j.cemconcomp.2020.103855.
[11] V. Mechtcherine, K. van Tittelboom, A. Kazemian, E. Kreiger, B. Nematollahi, V. N. Nerella, M. Santhanam, G. de Schutter, G. Van Zijl, D. Lowke, E. Ivaniuk, M. Taubert, F. Bos, A roadmap for quality control of hardening and hardened printed concrete, Cem. Concr. Res. 157 (2022) 106800, https://doi.org/10.1016/J.CEMCONRES.2022.106800.
[12] U.M. Angst, B. Elsener, The size effect in corrosion greatly influences the predicted life span of concrete infrastructures, Sci. Adv. 3 (2017), https://doi.org/10.1126/SCIADV.1700751/SUPPL_FILE/1700751_SM.PDF.
[13] L. Li, A.A. Sagüés, Chloride corrosion threshold of reinforcing steel in alkaline solutions—effect of specimen size, Corrosion 60 (2004) 195–202, https://doi.org/10.5006/1.3287721.
[14] K. Pasupathy, S. Ramakrishnan, J. Sanjayan, Enhancing the properties of foam concrete 3D printing using porous aggregates, Cem. Concr. Compos. 133 (2022) 104687, https://doi.org/10.1016/J.CEMCONCOMP.2022.104687.
[15] P. Sikora, M. Techman, K. Federowicz, A.M. El-Khayatt, H.A. Saudi, M. Abd Elrahman, M. Hoffmann, D. Stephan, S.Y. Chung, Insight into the microstructural and durability characteristics of 3D printed concrete: cast versus printed specimens, Case Stud. Constr. Mater. 17 (2022) e01320, https://doi.org/10.1016/J.CSCM.2022.E01320.
[16] A.V. Rahul, M. Santhanam, H. Meena, Z. Ghani, Mechanical characterization of 3D printable concrete, Constr. Build. Mater. 227 (2019) 116710, https://doi.org/10.1016/j.conbuildmat.2019.116710.
[17] M. Bekaert, K. Van Tittelboom, G. De Schutter, The effect of curing conditions on the service life of 3D printed concrete formwork, Materials 16 (2023) 6972, https://doi.org/10.3390/MA16216972.
[18] B. Nematollahi, P. Vijay, J. Sanjayan, A. Nazari, M. Xia, V.N. Nerella, V. Mechtcherine, Effect of polypropylene fibre addition on properties of geopolymers made by 3D printing for digital construction, Materials 11 (2018) 2352, https://doi.org/10.3390/ma11122352.
[19] J. Van Der Putten, M. Deprez, V. Cnudde, G. De Schutter, K. Van Tittelboom, Microstructural characterization of 3D printed cementitious materials, Materials 12 (2019) 1–22, https://doi.org/10.3390/ma12182993.
[20] M.K. Mohan, A.V. Rahul, J.F. Van Stappen, V. Cnudde, G. De Schutter, K. Van Tittelboom, Assessment of pore structure characteristics and tortuosity of 3D printed concrete using mercury intrusion porosimetry and X-ray tomography, Cem. Concr. Compos. 140 (2023) 105104, https://doi.org/10.1016/J.CEMCONCOMP.2023.105104.
[21] D. Lowke, D. Talke, I. Dressler, D. Weger, C. Gehlen, C. Ostertag, R. Rael, Particle bed 3D printing by selective cement activation – applications, material and process technology, Cem. Concr. Res. 134 (2020) 106077, https://doi.org/10.1016/J.CEMCONRES.2020.106077.
[22] Y. Tao, A.V. Rahul, K. Lesage, K. Van Tittelboom, Y. Yuan, G. De Schutter, Mechanical and microstructural properties of 3D printable concrete in the context of the twin-pipe pumping strategy, Cem. Concr. Compos. 125 (2022) 104324, https://doi.org/10.1016/J.CEMCONCOMP.2021.104324.
[23] S. Yu, M. Xia, J. Sanjayan, L. Yang, J. Xiao, H. Du, Microstructural characterization of 3D printed concrete, J. Build. Eng. 44 (2021) 102948, https://doi.org/10.1016/J.JOBE.2021.102948.
[24] M.K. Mohan, A.V. Rahul, G. De Schutter, Interlayer Bond and Porosity of 3D Printed Concrete, in: RILEM Bookseries, 2021, pp. 1–10.
[25] M.K. Mohan, A.V. Rahul, G. De Schutter, K. Van Tittelboom, Salt Scaling Resistance of 3D Printed Concrete, in: RILEM Bookseries, 37, 2022, pp. 188–193, https://doi.org/10.1007/978-3-031-06116-5_28/FIGURES/3.
[26] Y. Zhang, Y. Zhang, L. Yang, G. Liu, Y. Chen, S. Yu, H. Du, Hardened properties and durability of large-scale 3D printed cement-based materials, Mater. Struct./Mater. Constr. 54 (2021) 1–14, https://doi.org/10.1617/S11527-021-01632-X/FIGURES/11.
[27] K. Scrivener, R. Snellings, B. Lothenbach, A practical guide to microstructural analysis of cementitious materials, n.d. https://www.routledge.com/A-Practical-Guide-to-Microstructural-Analysis-of-Cementitious-Materials/Scrivener-Snellings-Lothenbach/p/book/9781138747234 (accessed December 19, 2023).
[28] A.C.A. Muller, K.L. Scrivener, A reassessment of mercury intrusion porosimetry by comparison with 1H NMR relaxometry, Cem. Concr. Res. 100 (2017) 350–360, https://doi.org/10.1016/J.CEMCONRES.2017.05.024.
[29] F. Thérèné, E. Keita, J. Naël-Redolfi, P. Boustingorry, L. Bonafous, N. Roussel, Water absorption of recycled aggregates: measurements, influence of temperature and practical consequences, Cem. Concr. Res. 137 (2020) 106196, https://doi.org/10.1016/J.CEMCONRES.2020.106196.
[30] Y. Chen, O. Çopuroğlu, C. Romero Rodriguez, F.F. de Mendonca Filho, E. Schlangen, Characterization of air-void systems in 3D printed cementitious materials using optical image scanning and X-ray computed tomography, Mater. Charact. 173 (2021) 110948, https://doi.org/10.1016/j.matchar.2021.110948.
[31] T.T. Le, S.A. Austin, S. Lim, R.A. Buswell, R. Law, A.G.F. Gibb, T. Thorpe, Hardened properties of high-performance printing concrete, Cem. Concr. Res. 42 (2012) 558–566, https://doi.org/10.1016/j.cemconres.2011.12.003.
[32] V.N. Nerella, S. Hempel, V. Mechtcherine, Effects of layer-interface properties on mechanical performance of concrete elements produced by extrusion-based 3D-printing, Constr. Build. Mater. 205 (2019) 586–601, https://doi.org/10.1016/j.conbuildmat.2019.01.235.

[33] L. He, H. Li, W.T. Chow, B. Zeng, Y. Qian, Increasing the interlayer strength of 3D printed concrete with tooth-like interface: an experimental and theoretical investigation, Mater. Des. 223 (2022) 111117, https://doi.org/10.1016/J.MATDES.2022.111117.

[34] J. Van Der Putten, M. De Volder, P. Van den Heede, M. Deprez, V. Cnudde, G. De Schutter, K. Van Tittelboom, Transport properties of 3D printed cementitious materials with prolonged time gap between successive layers, Cem. Concr. Res. 155 (2022) 106777, https://doi.org/10.1016/J.CEMCONRES.2022.106777.

[35] Y. Chen, Z. Chang, S. He, O. Çopuroğlu, B. Šavija, E. Schlangen, Effect of curing methods during a long time gap between two printing sessions on the interlayer bonding of 3D printed cementitious materials, Constr. Build. Mater. 332 (2022) 127394, https://doi.org/10.1016/j.conbuildmat.2022.127394.

[36] E. Keita, H. Bessaies-Bey, W. Zuo, P. Belin, N. Roussel, Weak bond strength between successive layers in extrusion-based additive manufacturing: measurement and physical origin, Cem. Concr. Res. 123 (2019) 105787, https://doi.org/10.1016/j.cemconres.2019.105787.

[37] S. Brisard, M. Serdar, P.J.M. Monteiro, Multiscale X-ray tomography of cementitious materials: a review, Cem. Concr. Res. 128 (2020) 105824, https://doi.org/10.1016/J.CEMCONRES.2019.105824.

[38] Z. Deng, Z. Jia, C. Zhang, Z. Wang, L. Jia, L. Ma, X. Wang, Y. Zhang, 3D printing lightweight aggregate concrete prepared with shell-packing-aggregate method - printability, mechanical properties and pore structure, J. Build. Eng. 62 (2022) 105404, https://doi.org/10.1016/J.JOBE.2022.105404.

[39] Y. Zhang, Y. Zhang, L. Yang, G. Liu, H. Du, Evaluation of aggregates, fibers and voids distribution in 3D printed concrete, J. Sustain. Cem.-Based Mater. 12 (2023) 775–788, https://doi.org/10.1080/21650373.2022.2113168.

[40] C. Liu, R. Zhang, H. Liu, C. He, Y. Wang, Y. Wu, S. Liu, L. Song, F. Zuo, Analysis of the mechanical performance and damage mechanism for 3D printed concrete based on pore structure, Constr. Build. Mater. 314 (2022) 125572, https://doi.org/10.1016/J.CONBUILDMAT.2021.125572.

[41] J. Kruger, A. du Plessis, G. van Zijl, An investigation into the porosity of extrusion-based 3D printed concrete, Addit. Manuf. 37 (2021) 101740, https://doi.org/10.1016/j.addma.2020.101740.

[42] M. van den Heever, A. du Plessis, J. Kruger, G. van Zijl, Evaluating the effects of porosity on the mechanical properties of extrusion-based 3D printed concrete, Cem. Concr. Res. 153 (2022) 106695, https://doi.org/10.1016/J.CEMCONRES.2021.106695.

[43] Z. Geng, W. She, W. Zuo, K. Lyu, H. Pan, Y. Zhang, C. Miao, Layer-interface properties in 3D printed concrete: dual hierarchical structure and micromechanical characterization, Cem. Concr. Res. 138 (2020) 106220, https://doi.org/10.1016/J.CEMCONRES.2020.106220.

[44] X. Huang, W. Yang, F. Song, J. Zou, Study on the mechanical properties of 3D printing concrete layers and the mechanism of influence of printing parameters, Constr. Build. Mater. 335 (2022) 127496, https://doi.org/10.1016/J.CONBUILDMAT.2022.127496.

[45] R. Yang, Q. Zeng, Y. Peng, H. Wang, Z. Wang, Anomalous matrix and interlayer pore structure of 3D-printed fiber-reinforced cementitious composites, Cem. Concr. Res. 157 (2022) 106829, https://doi.org/10.1016/J.CEMCONRES.2022.106829.

[46] R. Yang, Y. Zhu, Y. Lan, Q. Zeng, Y. Peng, Z. Wang, Differences in micro grain/fiber distributions between matrix and interlayer of cementitious filaments affected by extrusion molding, Addit. Manuf. 60 (2022) 103236, https://doi.org/10.1016/J.ADDMA.2022.103236.

[47] H. Liu, C. Liu, Y. Wu, G. Bai, C. He, Y. Yao, R. Zhang, Y. Wang, 3D printing concrete with recycled coarse aggregates: the influence of pore structure on interlayer adhesion, Cem. Concr. Compos. 134 (2022) 104742, https://doi.org/10.1016/J.CEMCONCOMP.2022.104742.

[48] L. Du, J. Zhou, J. Lai, K. Wu, X. Yin, Y. He, Effect of pore structure on durability and mechanical performance of 3D printed concrete, Constr. Build. Mater. 400 (2023) 132581, https://doi.org/10.1016/J.CONBUILDMAT.2023.132581.

[49] A. Cicione, J. Kruger, R.S. Walls, G. Van Zijl, An experimental study of the behavior of 3D printed concrete at elevated temperatures, Fire Saf. J. 120 (2021) 103075, https://doi.org/10.1016/j.firesaf.2020.103075.

[50] H. Lee, J.H.J. Kim, J.H. Moon, W.W. Kim, E.A. Seo, Correlation between pore characteristics and tensile bond strength of additive manufactured mortar using X-ray computed tomography, Constr. Build. Mater. 226 (2019) 712–720, https://doi.org/10.1016/J.CONBUILDMAT.2019.07.161.

[51] H. Kloft, H.W. Krauss, N. Hack, E. Herrmann, S. Neudecker, P.A. Varady, D. Lowke, Influence of process parameters on the interlayer bond strength of concrete elements additive manufactured by Shotcrete 3D Printing (SC3DP), Cem. Concr. Res. 134 (2020) 106078, https://doi.org/10.1016/j.cemconres.2020.106078.

[52] Y. Chen, J. Kuva, A. Mohite, Z. Li, H. Rahier, F. Al-Neshawy, J. Shu, Investigation of the internal structure of hardened 3D-printed concrete by X-CT scanning and its influence on the mechanical performance, Materials 16 (2023) 2534, https://doi.org/10.3390/MA16062534.

[53] R.A. Ketcham, W.D. Carlson, Acquisition, optimization and interpretation of X-ray computed tomographic imagery: applications to the geosciences, Comput. Geosci. 27 (2001) 381–400, https://doi.org/10.1016/S0098-3004(00)00116-3.

[54] M. Taleb, D. Bulteel, D. Betrancourt, F. Roudet, S. Rémond, D. Chicot, Interfacial weakness criterion by indentation in 3D printed concrete, 3D, Print. Addit. Manuf. 10 (2023) 318–329, https://doi.org/10.1089/3DP.2021.0128.

[55] M. Taleb, D. Bulteel, D. Betrancourt, F. Roudet, S. Rémond, A. Montagne, D. Chicot, Multi-scale mechanical characterization of the interface in 3D printed concrete, Mater. Struct./Mater. Constr. 56 (2023) 1–16, https://doi.org/10.1617/S11527-023-02114-Y/FIGURES/14.

[56] M. Kosson, L. Brown, F. Sanchez, Nanomechanical characterization of 3D printed cement pastes, J. Build. Eng. 66 (2023) 105874, https://doi.org/10.1016/J.JOBE.2023.105874.

[57] J. De'M Malan, A.S. van Rooyen, G.P.A.G. van Zijl, Chloride induced corrosion and carbonation in 3D printed concrete, Infrastructures 7 (2021) 1, https://doi.org/10.3390/INFRASTRUCTURES7010001, 2022, Vol. 7, Page 1.

[58] A.M.A. Sanchez, T. Wangler, M. Stefanoni, U. Angst, Microstructural examination of carbonated 3D-printed concrete, J. Microsc. 286 (2022) 141–147, https://doi.org/10.1111/JMI.13087.

[59] P. Bran-Anleu, T. Wangler, V.N. Nerella, V. Mechtcherine, P. Trtik, R.J. Flatt, Using micro-XRF to characterize chloride ingress through cold joints in 3D printed concrete, Mater. Struct./Mater. Constr. 56 (2023), https://doi.org/10.1617/s11527-023-02132-w.

[60] P. Bran-Anleu, F. Caruso, T. Wangler, E. Pomjakushina, R.J. Flatt, Standard and sample preparation for the micro XRF quantification of chlorides in hardened cement pastes, Microchem. J. 141 (2018) 382–387, https://doi.org/10.1016/J.MICROC.2018.05.040.

[61] C. Schröfl, V.N. Nerella, V. Mechtcherine, Capillary water intake by 3D-printed concrete visualised and quantified by neutron radiography, in: RILEM Bookseries, Springer Netherlands, 2019, pp. 217–224, https://doi.org/10.1007/978-3-319-99519-9_20.

[62] D. Feys, Interactions Between Rheological Properties and Pumping of Self-compacting Concrete, Doctoral Dissertation, Ghent University, 2009.

[63] ACI 305R-99, Hot Weather Concreting, 2000.

[64] L. Ma, Q. Zhang, Z. Jia, C. Liu, Z. Deng, Y. Zhang, Effect of drying environment on mechanical properties, internal RH and pore structure of 3D printed concrete, Constr. Build. Mater. 315 (2022) 125731, https://doi.org/10.1016/J.CONBUILDMAT.2021.125731.

[65] Y. Zhang, H. Qiao, R. Qian, C. Xue, Q. Feng, L. Su, Y. Zhang, G. Liu, H. Du, Relationship between water transport behaviour and interlayer voids of 3D printed concrete, Constr. Build. Mater. 326 (2022) 126731, https://doi.org/10.1016/J.CONBUILDMAT.2022.126731.

[66] J. Van Der Putten, G. De Schutter, K. Van Tittelboom, The effect of print parameters on the (micro)structure of 3D printed cementitious materials, in: RILEM Bookseries, Springer Netherlands, 2019, pp. 234–244, https://doi.org/10.1007/978-3-319-99519-9_22.

[67] M.K. Mohan, A.V. Rahul, Y. Villagran-Zaccardi, G. De Schutter, K. Van Tittelboom, A rheometric approach to assess plastic shrinkage and implications of early age drying on the microstructure of cement-based materials, Cem. Concr. Res. 180 (2024) 107504, https://doi.org/10.1016/J.CEMCONRES.2024.107504.

[68] E. Keita, Y. Rifaai, P. Belin, N. Roussel, Influence of non-adsorbing polymers on drying of fresh mortars, Cem. Concr. Res. 116 (2019) 38–44, https://doi.org/10.1016/j.cemconres.2018.10.016.

[69] P. Lura, B. Pease, G.B. Mazzotta, F. Rajabipour, J. Weiss, Influence of shrinkage-reducing admixtures on development of plastic shrinkage cracks, ACI Mater. J. 104 (2007) 187–194, https://doi.org/10.14359/18582.

[70] F. Rajabipour, G. Sant, J. Weiss, Interactions between shrinkage reducing admixtures (SRA) and cement paste's pore solution, Cem. Concr. Res. 38 (2008) 606–615, https://doi.org/10.1016/j.cemconres.2007.12.005.

[71] M.K. Mohan, R.G. Pillai, M. Santhanam, R. Gettu, High-performance cementitious grout with fly ash for corrosion protection of post-tensioned concrete structures, Constr. Build. Mater. 281 (2021) 122612, https://doi.org/10.1016/j.conbuildmat.2021.122612.

[72] A.V. Rahul, M.K. Mohan, G. De Schutter, K. Van Tittelboom, Assessment of early-age drying induced microstructural changes in 3D printed cement mortar, in: ICCC2023, 2023.

[73] N. Roussel, Rheological requirements for printable concretes, Cem. Concr. Res. 112 (2018) 76–85, https://doi.org/10.1016/j.cemconres.2018.04.005.

[74] F. Bos, R. Wolfs, Z. Ahmed, T. Salet, Additive manufacturing of concrete in construction: potentials and challenges of 3D concrete printing, Virtual Phys. Prototyp. 11 (2016) 209–225, https://doi.org/10.1080/17452759.2016.1209867.

[75] EN 13057, Products and Systems for the Protection and Repair of Concrete Structures - Test Methods - Determination of Resistance of Capillary Absorption, 2002.

[76] J. Van Der Putten, M. Azima, P. Van den Heede, T. Van Mullem, D. Snoeck, C. Carminati, J. Hovind, P. Trtik, G. De Schutter, K. Van Tittelboom, Neutron radiography to study the water ingress via the interlayer of 3D printed cementitious materials for continuous layering, Constr. Build. Mater. 258 (2020) 130–137, https://doi.org/10.1016/j.conbuildmat.2020.119587.

[77] J. Van Steenkiste, T. Wauters, Development of Test Methods for the Sustainability Assessment of 3D Printed Concrete, Master's thesis, Ghent University, 2023.

[78] M.B. Jaji, K.A. Ibrahim, G.P.A.G. van Zijl, A.J. Babafemi, Effect of anisotropy on permeability index and water absorption of 3D printed metakaolin-based geopolymer concrete, Mater. Today Proc. (2023), https://doi.org/10.1016/J.MATPR.2023.06.394.

[79] SANS-3001-CO3-1, Civil Engineering Test Methods: Part CO3-1: Concrete Durability Index Testing - Preparation of Test Specimens, Pretoria, 2015.

[80] SANS-3001-CO3-2, Civil Engineering Test Methods: Part CO3-2: Durability Index Testing-oxygen Permeability Test, Pretoria, 2015.

[81] V. Shah, S. Bishnoi, Carbonation resistance of cements containing supplementary cementitious materials and its relation to various parameters of concrete, Constr. Build. Mater. 178 (2018) 219–232, https://doi.org/10.1016/J.CONBUILDMAT.2018.05.162.

[82] J.H.M. Visser, Influence of the carbon dioxide concentration on the resistance to carbonation of concrete, Constr. Build. Mater. 67 (2014) 8–13, https://doi.org/10.1016/J.CONBUILDMAT.2013.11.005.
[83] J. Van Der Putten, Mechanical Properties and Durability of 3D Printed Cementitious Materials, 2021.
[84] M. Elsalamawy, A.R. Mohamed, E.M. Kamal, The role of relative humidity and cement type on carbonation resistance of concrete, Alex. Eng. J. 58 (2019) 1257–1264, https://doi.org/10.1016/J.AEJ.2019.10.008.
[85] G.M. Moelich, P.J. Kruger, R. Combrinck, The effect of restrained early age shrinkage on the interlayer bond and durability of 3D printed concrete, J. Build. Eng. 43 (2021) 102857, https://doi.org/10.1016/j.jobe.2021.102857.
[86] S. Surehali, A. Tripathi, A.S. Nimbalkar, N. Neithalath, Anisotropic chloride transport in 3D printed concrete and its dependence on layer height and interface types, Addit. Manuf. 62 (2023) 103405, https://doi.org/10.1016/J.ADDMA.2023.103405.
[87] NT Build 492, Concrete, Mortar and Cement-based Repair Materials: Chloride Migration Coefficient From Non-steady-state Migration Experiments, 1999.
[88] L. Wang, W. Xiao, Q. Wang, H. Jiang, G. Ma, Freeze-thaw resistance of 3D-printed composites with desert sand, Cem. Concr. Compos. 133 (2022) 104693, https://doi.org/10.1016/J.CEMCONCOMP.2022.104693.
[89] R. Maria Ghantous, A. Evseeva, B. Dickey, S. Gupta, A. Prihar, H.S. Esmaeeli, R. Moini, W.J. Weiss, Examining effect of printing directionality on the freezing-and-thawing response of three-dimensional-printed cement paste, ACI Mater. J. 120 (2023) 89–102, https://doi.org/10.14359/51738808.
[90] J.J. Assaad, F. Hamzeh, B. Hamad, Qualitative assessment of interfacial bonding in 3D printing concrete exposed to frost attack, Case Stud. Constr. Mater. 13 (2020) e00357, https://doi.org/10.1016/j.cscm.2020.e00357.
[91] A. Das, Y. Song, S. Mantellato, T. Wangler, D.A. Lange, R.J. Flatt, Effect of processing on the air void system of 3D printed concrete, Cem. Concr. Res. 156 (2022) 106789, https://doi.org/10.1016/J.CEMCONRES.2022.106789.
[92] T. Wangler, A.M. Aguilar Sanchez, A. Anton, B. Dillenburger, R.J. Flatt, Two Year Exposure of 3D Printed Cementitious Columns in a High Alpine Environment, in: RILEM Bookseries, 37, 2022, pp. 182–187, https://doi.org/10.1007/978-3-031-06116-5_27/FIGURES/4.
[93] ASTM C 666, Standard Test Method for Resistance of Concrete to Rapid Freezing and Thawing, West Conshohocken, www.astm.org, 2008.
[94] J.J. Valenza, G.W. Scherer, A review of salt scaling: I. Phenomenology, Cem. Concr. Res. 37 (2007) 1007–1021, https://doi.org/10.1016/j.cemconres.2007.03.005.
[95] CEN / TS 12390-9, PKN-CEN/TS 12390-9:2017-07 Testing Hardened Concrete - Part 9: Freeze-thaw Resistance With De-icing Salts - Scaling, 2017.
[96] A. Rui, L. Wang, W. Lin, G. Ma, Experimental study on damage anisotropy of 3D-printed concrete exposed to sulfate attack, Constr. Build. Mater. 407 (2023) 133590, https://doi.org/10.1016/J.CONBUILDMAT.2023.133590.
[97] B. Baz, G. Aouad, J. Kleib, D. Bulteel, S. Remond, Durability assessment and microstructural analysis of 3D printed concrete exposed to sulfuric acid environments, Constr. Build. Mater. 290 (2021) 123220, https://doi.org/10.1016/J.CONBUILDMAT.2021.123220.
[98] GB/T 50082, Standard for Test Methods of Long-term Performance and Durability of Ordinary Concrete, 2009.
[99] ASTM C779, Standard Test Method for Abrasion Resistance of Horizontal Concrete Surfaces, West Conshohocken, www.astm.org, 2019.
[100] NBN EN 13892-4:2002, Methods of Test for Screed Materials - Part 4: Determination of Wear Resistance-BCA. www.bin.be, 2003.
[101] BS EN 13892-3:2014, Methods of test for screed materials - Part 3: Determination of wear resistance - Böhme., n.d.
[102] D.S. Kurup, M.K. Mohan, K. Van Tittelboom, G. De Schutter, M. Santhanam, A. V. Rahul, Early-age shrinkage assessment of cementitious materials: a critical review, Cem. Concr. Compos. 145 (2024) 105343, https://doi.org/10.1016/J.CEMCONCOMP.2023.105343.
[103] G.M. Moelich, J. Kruger, R. Combrinck, Plastic shrinkage cracking in 3D printed concrete, Compos. B Eng. 200 (2020) 108313, https://doi.org/10.1016/j.compositesb.2020.108313.
[104] G.M. Moelich, P.J. Kruger, R. Combrinck, A plastic shrinkage cracking risk model for 3D printed concrete exposed to different environments, Cem. Concr. Compos. 130 (2022) 104516, https://doi.org/10.1016/j.cemconcomp.2022.104516.
[105] S. Markin, V. Mechtcherine, Quantification of plastic shrinkage and plastic shrinkage cracking of the 3D printable concretes using 2D digital image correlation, Cem. Concr. Compos. 139 (2023) 105050, https://doi.org/10.1016/J.CEMCONCOMP.2023.105050.
[106] J.L. Tao, C. Lin, Q.L. Luo, W.J. Long, S.Y. Zheng, C.Y. Hong, Leveraging internal curing effect of fly ash cenosphere for alleviating autogenous shrinkage in 3D printing, Constr. Build. Mater. 346 (2022) 128247, https://doi.org/10.1016/J.CONBUILDMAT.2022.128247.
[107] H. Zhang, L. Hao, S. Zhang, J. Xiao, C.S. Poon, Advanced measurement techniques for plastic shrinkage and cracking in 3D-printed concrete utilising distributed optical fiber sensor, Addit. Manuf. 74 (2023) 103722, https://doi.org/10.1016/J.ADDMA.2023.103722.
[108] A.H. Buchanan, A. Abu, Structural Design for Fire Safety, Second, John Wiley & Sons, 2017.
[109] FIP-CEB, High Strength Concrete - Joint FIP/CEB State-of-the-art Report, London, 1990.
[110] R.B. Figueira, R. Sousa, L. Coelho, M. Azenha, J.M. de Almeida, P.A.S. Jorge, C.J. R. Silva, Alkali-silica reaction in concrete: mechanisms, mitigation and test methods, Constr. Build. Mater. 222 (2019) 903–931, https://doi.org/10.1016/J.CONBUILDMAT.2019.07.230.
[111] M. Thomas, B. Fournier, K. Folliard, J. Ideker, M. Shehata, Test methods for evaluating preventive measures for controlling expansion due to alkali–silica reaction in concrete, Cem. Concr. Res. 36 (2006) 1842–1856, https://doi.org/10.1016/J.CEMCONRES.2006.01.014.
[112] C. Paglia, F. Wombacher, H. Böhni, The influence of alkali-free and alkaline shotcrete accelerators within cement systems: influence of the temperature on the sulfate attack mechanisms and damage, Cem. Concr. Res. 33 (2003) 387–395, https://doi.org/10.1016/S0008-8846(02)00967-5.
[113] C. Ouyang, A. Nanni, W.F. Chang, Internal and external sources of sulfate ions in portland cement mortar: two types of chemical attack, Cem. Concr. Res. 18 (1988) 699–709, https://doi.org/10.1016/0008-8846(88)90092-0.
[114] A.U. Rehman, B.M. Birru, J.H. Kim, Set-on-demand 3D Concrete Printing (3DCP) construction and potential outcome of shotcrete accelerators on its hardened properties, Case Stud. Constr. Mater. 18 (2023) e01955, https://doi.org/10.1016/J.CSCM.2023.E01955.
[115] L. Wang, Y. Yang, L. Yao, G. Ma, Interfacial bonding properties of 3D printed permanent formwork with the post-casted concrete, Cem. Concr. Compos. 128 (2022) 104457, https://doi.org/10.1016/j.cemconcomp.2022.104457.
[116] M. Bekaert, K. Van Tittelboom, G. De Schutter, 3D printed concrete as stay-in-place formwork: mechanics during casting and curing, Struct. Concr. (2022), https://doi.org/10.1002/suco.202200088.
[117] L. Dong, Y. Yang, Z. Liu, Q. Ren, J. Li, Y. Zhang, C. Wu, Microstructure and mechanical behaviour of 3D printed ultra-high performance concrete after elevated temperatures, Addit. Manuf. 58 (2022) 103032, https://doi.org/10.1016/J.ADDMA.2022.103032.
[118] A.R. Arunothayan, J.G. Sanjayan, Elevated temperature effects on 3D printed ultra-high performance concrete, Constr. Build. Mater. 367 (2023) 130241, https://doi.org/10.1016/J.CONBUILDMAT.2022.130241.
[119] J. Xiao, N. Han, L. Zhang, S. Zou, Mechanical and microstructural evolution of 3D printed concrete with polyethylene fiber and recycled sand at elevated temperatures, Constr. Build. Mater. 293 (2021) 123524, https://doi.org/10.1016/J.CONBUILDMAT.2021.123524.
[120] T. Suntharalingam, I. Upasiri, B. Nagaratnam, K. Poologanathan, P. Gatheeshgar, K.D. Tsavdaridis, D. Nuwanthika, Finite element modelling to predict the fire performance of bio-inspired 3D-printed concrete wall panels exposed to realistic fire, Buildings 12 (2022) 111, https://doi.org/10.3390/BUILDINGS12020111.
[121] T. Ooms, G. Vantyghem, T. Thienpont, R. Van Coile, W. De Corte, Thermoelastic topology optimization of structural components at elevated temperatures considering transient heat conduction, Eng. Comput. (2023), https://doi.org/10.1007/s00366-023-01907-7.
[122] L. Wang, W. Lin, H. Ma, D. Li, Q. Wang, Mechanical and microstructural properties of 3D-printed aluminate cement based composite exposed to elevated temperatures, Constr. Build. Mater. 353 (2022) 129144, https://doi.org/10.1016/J.CONBUILDMAT.2022.129144.
[123] G.M. Moelich, P.J. Kruger, R. Combrinck, Mitigating early age cracking in 3D printed concrete using fibres, superabsorbent polymers, shrinkage reducing admixtures, B-CSA cement and curing measures, Cem. Concr. Res. 159 (2022) 106862, https://doi.org/10.1016/j.cemconres.2022.106862.
[124] J. Van Der Putten, D. Snoeck, R. De Coensel, G. De Schutter, K. Van Tittelboom, Early age shrinkage phenomena of 3D printed cementitious materials with superabsorbent polymers, J. Build. Eng. 35 (2021) 102059, https://doi.org/10.1016/J.JOBE.2020.102059.
[125] H. Yao, Z. Xie, Z. Li, C. Huang, Q. Yuan, X. Zheng, The relationship between the rheological behavior and interlayer bonding properties of 3D printing cementitious materials with the addition of attapulgite, Constr. Build. Mater. 316 (2022) 125809, https://doi.org/10.1016/J.CONBUILDMAT.2021.125809.
[126] G.M. Moelich, J. Kruger, R. Combrinck, Modelling the interlayer bond strength of 3D printed concrete with surface moisture, Cem. Concr. Res. 150 (2021) 106559, https://doi.org/10.1016/J.CEMCONRES.2021.106559.
[127] G.M. Moelich, J.J. Janse van Rensburg, J. Kruger, R. Combrinck, The Environment's Effect on the Interlayer Bond Strength of 3D Printed Concrete, in: RILEM Bookseries, 37, 2022, pp. 222–227, https://doi.org/10.1007/978-3-031-06116-5_33/FIGURES/3.
[128] J. Kruger, S. Cho, S. Zeranka, C. Viljoen, G. van Zijl, 3D concrete printer parameter optimisation for high rate digital construction avoiding plastic collapse, Compos. B Eng. 183 (2020) 107660, https://doi.org/10.1016/j.compositesb.2019.107660.
[129] J. Van Der Putten, G. De Schutter, K. Van Tittelboom, Surface modification as a technique to improve inter-layer bonding strength in 3d printed cementitious materials, RILEM Tech. Lett. 4 (2019) 33–38, https://doi.org/10.21809/rilemtechlett.2019.84.
[130] R. Munemo, J. Kruger, G.P.A.G. van Zijl, Improving interlayer bond in 3D printed concrete through induced thermo-hydrokinetics, Constr. Build. Mater. 393 (2023) 132121, https://doi.org/10.1016/J.CONBUILDMAT.2023.132121.
[131] Z. Geng, P. Wu, H. Pan, Q. Zheng, W. Zuo, W. Zhang, W. She, Robust layer interface in cement additive manufacturing via silicate penetration and precipitation, Mater. Des. 214 (2022) 110380, https://doi.org/10.1016/J.MATDES.2022.110380.
[132] G. Ma, N.M. Salman, L. Wang, F. Wang, A novel additive mortar leveraging internal curing for enhancing interlayer bonding of cementitious composite for 3D printing, Constr. Build. Mater. 244 (2020) 118305, https://doi.org/10.1016/j.conbuildmat.2020.118305.
[133] T. Marchment, J. Sanjayan, M. Xia, Method of enhancing interlayer bond strength in construction scale 3D printing with mortar by effective bond area amplification, Mater. Des. 169 (2019) 107684, https://doi.org/10.1016/j.matdes.2019.107684.

[134] L. Wang, Z. Tian, G. Ma, M. Zhang, Interlayer bonding improvement of 3D printed concrete with polymer modified mortar: experiments and molecular dynamics studies, Cem. Concr. Compos. 110 (2020) 103571, https://doi.org/10.1016/j.cemconcomp.2020.103571.

[135] E. Hosseini, M. Zakertabrizi, A.H. Korayem, G. Xu, A novel method to enhance the interlayer bonding of 3D printing concrete: an experimental and computational investigation, Cem. Concr. Compos. 99 (2019) 112–119, https://doi.org/10.1016/j.cemconcomp.2019.03.008.

[136] M.K. Mohan, A.V. Rahul, G. De Schutter, K. Van Tittelboom, Transport properties of 3D printed concrete elements, in: 76th Annual RILEM Week and the International Conference on Regeneration and Conservation of Structures (ICRCS 2022), Proceedings, 2022. http://hdl.handle.net/1854/LU-01GS7F4PXWZWV363MTSXJABVZ7. (Accessed 19 December 2023).

[137] J.P. Mostert, J. Kruger, Interlocking 3D Printed Concrete Filaments Through Surface Topology Modifications for Improved Tensile Bond Strength, in: RILEM Bookseries, 37, 2022, pp. 235–240, https://doi.org/10.1007/978-3-031-06116-5_35/FIGURES/4.

[138] Build Your Own 3D Printed House, All in One Day | ArchDaily, (n.d.). https://www.archdaily.com/806742/build-your-own-3d-printed-house-all-in-one-day?ad_medium=gallery (accessed February 7, 2024).

[139] The Most Innovative 3D Printed House in the World – Automate Construction, (n.d.). https://automateconstruction.com/2021/03/30/the-most-innovative-3d-printed-house-in-the-world/ (accessed February 6, 2024).

[140] Diamond Age | 3d Technology, (n.d.). https://www.diamondage3d.com/ (accessed February 6, 2024).

[141] Y. Weng, M. Li, T.N. Wong, M.J. Tan, Synchronized concrete and bonding agent deposition system for interlayer bond strength enhancement in 3D concrete printing, Autom. Constr. 123 (2021) 103546, https://doi.org/10.1016/j.autcon.2020.103546.

[142] A. AL-Ameeri, M. Rafiq, O. Tsioulo, Influence of Cracks on the Carbonation Resistance of Concrete Structures, International Conference on Durability of Concrete Structures. https://docs.lib.purdue.edu/icdcs/2018/pse/5, 2019. (Accessed 19 December 2023).

[143] K. Federowicz, M. Kaszyńska, A. Zieliński, M. Hoffmann, Effect of curing methods on shrinkage development in 3D-printed concrete, Materials 13 (2020) 2590, https://doi.org/10.3390/MA13112590.